Biochimica et Biophysica Acta 1807 (2011) 130–143

Contents lists available at ScienceDirect

Biochimica et Biophysica Acta

journal homepage: www.elsevier.com/locate/bbabio

Quantitative evaluation of the intrinsic uncoupling modulated by ADP and P_i in the reconstituted ATP synthase of *Escherichia coli*

Manuela D'Alessandro [1], Paola Turina *, B. Andrea Melandri

Department of Biology, Laboratory of Biochemistry and Biophysics, University of Bologna, Via Irnerio 42, 40126 Bologna, Italy

ARTICLE INFO

Article history:
Received 16 July 2010
Received in revised form 17 August 2010
Accepted 18 August 2010
Available online 26 August 2010

Keywords:
E. coli
ATP synthase
H^+/ATP
Coupling ratio
Intrinsic uncoupling
Proteoliposomes

ABSTRACT

The ATP synthase from *Escherichia coli* was isolated and reconstituted into liposomes. The ATP hydrolysis by these proteoliposomes was coupled to proton pumping, and the ensuing inner volume acidification was measured by the fluorescent probe 9-amino-6-chloro-2-methoxyacridine (ACMA). The ACMA response was calibrated by acid–base transitions, and converted into internal pH values. The rates of internal acidification and of ATP hydrolysis were measured in parallel, as a function of P_i or ADP concentration. Increasing P_i monotonically inhibited the hydrolysis rate with a half-maximal effect at 510 μM, whereas it stimulated the acidification rate up to 100–200 μM, inhibiting it only at higher concentrations. The ADP concentration in the assay, due both to contaminant ADP in ATP and to the hydrolysis reaction, was progressively decreased by means of increasing pyruvate kinase activities. Decreasing ADP stimulated the hydrolysis rate, whereas it inhibited the internal acidification rate. The quantitative analysis showed that the relative number of translocated protons per hydrolyzed ATP, i.e. the relative coupling ratio, depended on the concentrations of P_i and ADP with apparent K_d values of 220 μM and 27 nM respectively. At the smallest ADP concentrations reached, and in the absence of P_i, the coupling ratio dropped down to 15% relative to the value observed at the highest ADP and P_i concentrations tested. In addition, the data indicate the presence of two ADP and P_i binding sites, of which only the highest affinity one is related to changes in the coupling ratio.

1. Introduction

F_0F_1-ATPases or ATP synthases are highly conserved enzymes found in bacteria, mitochondria and chloroplasts, which catalyze ATP synthesis at the expense of a transmembrane electrochemical potential difference of protons (or Na^+ ions in some species) and can also work in the opposite direction, building up a proton (or Na^+) electrochemical potential difference at the expenses of ATP hydrolysis [1–5]. They are composed of a membrane embedded hydrophobic sector, F_0, through which proton translocation across the membrane occurs, constituted in its simplest form by 3 subunits in stoichiometry ab_2c_{10-15}, and of a hydrophilic extrinsic sector, F_1, which houses the catalytic sites, constituted in its simplest form by 5 subunits in stoichiometry $\alpha_3\beta_3\gamma\delta\varepsilon$. The structure of the whole complex remains as yet unresolved, but a high resolution structure of the bovine mitochondrial F_1 was achieved in 1994 [6]. Subsequently several additional structures of bovine F_1 have been obtained, in which the catalytic subunits exhibit different functional states induced by a variety of substrates, product analogues, or inhibitors [see e.g. 9–12]. Structures from chloroplast [13], *Escherichia coli* [14], and more recently from *Saccharomyces cerevisiae* F_1 [15] are also available. Comparison of these structures reveals the substantial close similarity of ATP synthase in all these organisms.

The structural data turned out to tie in extremely well with the functional model first proposed by Boyer [7,8], according to which the catalytic nucleotide binding sites on the β-subunits operated in a cyclic way, accomplished by a rotatory movement of the γ-subunit within the $\alpha_3\beta_3$-subunit hexamer. Plenty of experimental evidence has confirmed and enriched that model (reviewed in [2,4]). Besides the γ-subunit, rotor's component are the ε-subunit in F_1 and the *c*-subunit ring in F_0, whose rotary movement against the *a*-subunit of the stator is thought to be coupled to proton flow through F_0. In its simplest version, the model of rotatory catalysis implies that the coupling between proton flows through F_0 and the catalytic reactions at the nucleotide binding sites,

Abbreviations: EF_0F_1, ATP synthase of *E. coli*; EF_1, hydrophylic subcomplex of the ATP synthase of *E. coli*; Tris, (hydroxymethyl) aminomethane; DTT, dithiothreitol; PMSF, phenylmethylsulfonyl fluoride; p-ABA, p-aminobenzoic acid; MOPS, 3-(N-morpholino)propanesulfonic acid; OG, octyl β-D-glucopyranoside; Tricine, N-[2-hydroxy-1,1-bis(hydroxymethyl)ethyl] glycine; EDTA, ethylenediaminetetraacetic acid; PK, pyruvate kinase; PEP, phosphoenolpyruvate; LDH, lactate dehydrogenase; Phenol Red, 4,4'-(3H-2,1-benzoxathiol-3-ylidene) bis-phenol, S,S-dioxide; Δψ, bulk-to-bulk transmembrane electrical potential difference; ACMA, 9-amino-6-chloro-2-methoxyacridine; $\Delta\tilde{\mu}_{H^+}$, transmembrane difference of electrochemical potential of protons; ΔpH, transmembrane difference of pH ($pH_{out} - pH_{in}$)

* Corresponding author. Laboratory of Biochemistry and Biophysics, Department of Biology, University of Bologna, Via Irnerio, 42, I-40126 Bologna, Italy. Tel.: +39 051 2091322; fax: +39 051 242576.
E-mail address: paola.turina@unibo.it (P. Turina).
URL: http://www.biologia.unibo.it/ (P. Turina).
[1] Present address: Department of Neurobiology and Genetics I.G.B.M.C. 1, rue Laurent Fries B.P. 10142, 67404 Illkirch, France.

0005-2728/$ – see front matter © 2010 Elsevier B.V. All rights reserved.
doi:10.1016/j.bbabio.2010.08.011

both in the synthesis and hydrolysis direction, occurs with a fixed H^+/ATP stoichiometry. This notion stems from the concept that the central rotor of the enzyme rotates and interacts as a single solid body with the three catalytic sites in F_1 and that the number of protons translocated per rotor turn is strictly related to the number of *c*-subunits present in the F_0 sector.

However, the possibility of intrinsic uncoupling of mitochondrial redox and ATPase H^+-pumps, leading to an effective H^+/ATP coupling ratio lower than the H^+/ATP stoichiometry, has been the topic of theoretical work in the past [see e.g. [16]] and a variable ratio between phosphorylation potential and ion gradient potentials under different conditions had been reported e.g. in inverted *Rhodobacter capsulatus* membranes [17], in bovine heart submitochondrial particles [18], in *Bacillus licheniformis* cells [19], or in cells of a thermoalkaliphilic aerobic bacterium [20]. The idea of a variable coupling ratio in the *E. coli* enzyme had been put forward by [21,22]. In addition, variability in the coupling ratio, in a few cases dependent on the pH_{in} and pH_{out} values, has been repeatedly found for several V-ATPases [23–26], a class of enzymes closely related to ATP synthases.

Recently, we have found evidence, based on the comparison between rates of ΔpH formation and rates of ATP hydrolysis, that the effective coupling ratio of the ATP synthase of inverted membranes from *Rb. capsulatus* [27] and *E. coli* [28] can vary as a function of the concentration of the hydrolysis products ADP and P_i, i.e. that the ATP synthase can become intrinsically uncoupled. The range of ADP concentration within which the phenomenon could be observed was extremely low, which might explain why it had remained unnoticed for a long time.

In the present work, we have isolated the *E. coli* ATP synthase and reconstituted it into preformed liposomes. Such reconstituted system has allowed us to quantitatively evaluate the extent of the ADP- and P_i-induced modulation of coupling efficiency.

2. Materials and methods

2.1. Cell growth, membrane preparation, and EF_0F_1 isolation

Cells from the XL1Blue *E. coli* strain carrying the kanamycin resistance on the plasmid pNK1 (Stratagene) were grown in LB medium, and harvested at a late exponential phase. Fifteen grams cells (wet weight) were washed with 400 ml of Buffer A (50 mM Tris–HCl, pH 8.0), resuspended in 200 ml Buffer B (50 mM Tris–HCl, pH 8.0, 140 mM KCl, 1 mM DTT, 10% glycerol (v/v), 10 μg/ml DNase, 100 μM PMSF, 6 mM p-ABA) and disrupted at 138 Mpa (20,000 p.s.i.) in the French Press. Unbroken cells were removed by centrifugation at 16000 rpm and the remaining supernatant was centrifuged in a Beckman type 50.2 Ti rotor at 40000 rpm for 90 min to pellet inverted membranes.

EF_0F_1 was isolated essentially as described in [29,30]. Inverted membranes were suspended in 15 ml Buffer C (40 mM MOPS, pH 7.0, 2 mM $MgCl_2$, 5 mM thioglycerol). The protein concentration was measured by the Bradford method [31] and adjusted to 10 mg/ml. The mixture was incubated for 10 min on ice in the presence of 2% OG. The supernatant obtained by centrifugation at 34.000 rpm for 60 min at 4 °C was applied to a sucrose gradient (20–45%) containing Buffer D (Buffer C + 0.6% OG), and centrifuged in a Beckman type 50.2Ti rotor at 35.000 rpm for 14 h at 4 °C. The fractions containing ATP hydrolysis activity (measured as loss of absorbance at 340 nm per unit time in the following ATP regenerating assay: 20 mM Tricine, pH 7.5, 2 mM $MgCl_2$, 10 mM KCl, 1 mM ATP, 2 mM PEP, 0.15 mM NADH, 5 mM KCN, 25 U/ml LDH, 25 U/ml PK) were combined and stored at −80 °C. EF_0F_1 purity was 40%, as estimated by densitometric scanning of gels stained by Coomassie Brilliant Blue; its concentration was calculated by measuring the total protein concentration [31] and taking the purity factor into account, on the basis of a molecular mass of 550 kDa.

2.2. Liposome preparation and EF_0F_1 reconstitution

Liposomes from phosphatidylcholine and phosphatidic acid were prepared by dialysis as described in [32]. 18 g/l phosphatidylcholine and phosphatidic acid in a mass ratio of 19:1 were suspended in sonication buffer (10 mM Tricine/NaOH, pH 8, 0.5 mM DTT, 0.1 mM EDTA, containing 7.2 g/l cholic acid and 3.6 g/l sodium desoxycholate), sonicated in an ice bath for 3 × 30 s (Branson sonifier at 20 kHz and 150 W) and dialyzed against a 4000-fold volume of dialysis buffer (10 mM Tricine/NaOH, pH 8, 2.5 mM $MgCl_2$, 0.25 mM DTT, 0.2 mM EDTA) at room temperature overnight using a Diachema membrane type 10.14 MWC 5000. The lipid concentration after dialysis was approximately 16 g/l. Purified EF_0F_1 was reconstituted into these preformed liposomes essentially as described in [32,33]. Reconstitution assays contained, in a final volume of 200 μl: 100 μl liposome suspension, 20 mM succinate/20 mM Tricine/NaOH, pH 8.0, 3.75 mM $MgCl_2$ (2.5 + 1.25 from the dialysis buffer), 50 mM KCl (except for samples used in ATP synthesis measurements, which contained 0.5 mM KCl and 50 mM NaCl) and 0 to 0.30 μM purified EF_0F_1 in a total volume of 60 μl Buffer D. After addition of 0.65% (v/v) Triton X-100 and 60 min incubation at room temperature, the detergent was removed by incubating the suspension in the presence of 64 mg Bio-Beads SM-2 (extensively washed as described in [34]) for 60 min under gentle stirring. The resulting EF_0F_1 proteoliposomes could be stored at room temperature for up to 2 days without any loss of ATP synthesis activity.

2.3. ATP hydrolysis

All reactions were carried out in sample holders thermostated at 25 °C. ATP hydrolysis was measured either by detecting the scalar protons released upon ATP hydrolysis by means of the colorimetric pH indicator Phenol Red, or by measuring the rephosphorylation of the produced ADP by coupling the pyruvate kinase (PK) reaction to NADH oxidation via lactic dehydrogenase (LDH). The second method worked simultaneously as an ADP trap, and the extent to which the ADP was withdrawn could be modulated by the concentration of added PK. In the colorimetric proton detection assay, proteoliposomes were suspended to the desired EF_0F_1 concentration (routinely 3.0 nM), 15 min prior to the reaction start, in the following buffer: 1 mM Tricine, 50 mM KCl, 2.0 mM $MgCl_2$, NaOH to pH 8.0 (adjusted immediately prior to each measurements), 100 μM Phenol Red, and 1 μM valinomycin to minimize Δφ. The pH changes of the suspension were followed as a function of time in the double wavelength setup of a Jasco V-550 spectrophotometer by the absorbance changes at 625–587 nm. The absorbance changes were calibrated after about 200 s of reaction by 3 sequential addition of 15 μM HCl. The overall pH change of the suspension at the end of the measurements was never higher than 0.3 units. The calibration signals showed that the addition of 3 mM P_i in the poorly buffered assay medium caused a less than 2-fold increase of the buffering power. The changes of proton concentration were transformed to changes of ATP concentration as described [35]. At pH 8.0 a ratio for scalar proton to hydrolysed ATP equal to 0.94 was used. When ATP hydrolysis was measured by the ADP rephosphorylation method, the reaction conditions were the same, except that the suspension contained, instead of Phenol Red, 2 mM PEP, PK to variable amounts as indicated, 25 U/ml of LDH, and 0.15 mM NADH. The PK was supplied from Sigma (P-9136) as an ion-free lyophilized powder. The ADP rephosphorylation, coupled stoichiometrically to NADH oxidation, was followed by the absorbance changes at 340 nm as a function of time in the Jasco V-550 spectrophotometer. In isolated *E. coli* membranes it has been shown that the rates of ATP hydrolysis as measured either by the Phenol Red assay (in the absence of P_i) or by the malachite green assay [36] did not differ in the range of experimental error, and similarly that the hydrolysis rates in the presence of PK, PEP, LDH, NADH, and absence of P_i, did not differ significantly if measured either by the ADP rephosphorylation assay or by the malachite green assay [28].

2.4. ACMA assay and calibration

ACMA (Molecular Probes. Inc., Eugene, Oregon, USA) was dissolved in ethanol to a final concentration of 1.5 mM. The ACMA assays were carried out at 25 °C under experimental conditions as close as possible to those used for ATP hydrolysis measurements. The ACMA fluorescence emission was recorded as a function of time (RC = 0.25 s) in a Jasco FP 500 spectrofluorometer (wavelength 412 and 482 nm for excitation and emission respectively). When the ACMA assays were compared to the proton detection hydrolysis assays, the reaction conditions were the same as used for those hydrolysis measurements, except that Phenol Red was omitted and 1.5 μM ACMA was added. When the ACMA assays were compared to the ADP rephosphorylation hydrolysis assays, the reaction conditions were the same as used for those hydrolysis measurements, except that LDH and NADH were omitted and 1.5 μM ACMA was added. In control measurements, addition of pyruvate up to 100 μM did not affect the quenching signals.

For ACMA calibration, transmembrane ΔpHs were artificially imposed on proteoliposomes by means of acid–base transitions, following the procedure described in [37]. Various proteoliposome samples, suspended in a buffer containing 20 mM Tricine/20 mM succinate, pH 8.0, 50 mM KCl, 2 mM $MgCl_2$, 1 μM valinomycin, and 1.5 μM ACMA, were adjusted by addition of suitable volumes of 1 M HCl to pH values ranging from 4.2 to 8.0, and equilibrated for 30 min at 25 °C. Longer equilibration times, up to 2 h, did not change the subsequent fluorescence signal, indicating that full equilibration of proton concentration between the external and the intravesicular compartment had been reached. Therefore, the pH value during the equilibration time was taken as the internal pH value in the acid–base transition. The quenching of ACMA fluorescence as a function of time was recorded at the same temperature upon addition to the spectrofluorometer cuvette, by a Hamilton syringe and under vigorous stirring, of the same volumes of 1 M NaOH, so that the outside pH was brought rapidly (within about 0.5 s) to the constant value of 8.0. This procedure (acid–base transition) induced a transient transmembrane ΔpH (varying from 3.8 to 0 pH units) that was expected to decay due to the proton passive flow through the membrane. Correspondingly, a transient fluorescence quenching was observed, after which the original fluorescence intensity was recovered within several tens of seconds. The initial and final pH values of the suspensions were determined using a Radiometer PHM62 pHmeter, and their differences were taken as the imposed transmembrane ΔpH's. The maximum quenching values recorded upon the acid–base transition were taken as the ACMA fluorescence response to these calculated ΔpH values.

2.5. ATP synthesis

The rate of ATP synthesis catalyzed by EF_0F_1 was measured at 25 °C similarly as described in [30,32]. Proteoliposomes were energized by an acid/base transition in the presence of a K^+/valinomycin diffusion potential. ATP synthesis and detection of ATP with the luciferin/luciferase assay (Merlin) were carried out simultaneously in a luminometer (LKB 1250) as follows. 890 μl Buffer LII (200 mM Tricine, 160 mM KOH, 2 mM $MgCl_2$, 5 mM NaH_2PO_4, 0.1 mM ADP) were mixed with 10 μl luciferin/luciferase reagent, and the baseline was recorded. 30 μl of proteoliposomes (0 to 102 nM EF_0F_1) were mixed with 90 μl Buffer LI (20 mM succinate/NaOH, 0.5 mM KOH, pH 4.7, 2 mM $MgCl_2$, 5 mM NaH_2PO_4, 20 μM freshly added valinomycin) and incubated for 1–6 min. ATP synthesis was initiated by injection of 100 μl of this suspension (final pH 5.0) with a Hamilton syringe directly into the cuvette containing LII and luciferin/luciferase (final pH 8.5). The increase in luminescence was converted in increase of ATP concentration by adding 10 μl of an ATP solution of known concentration (10 μM) to calibrate the luminescence signal.

2.6. Measurement of pyruvate kinase activity and evaluation of the steady state ADP concentration in the ADP rephosphorylation assay

The activity of PK was measured under the experimental conditions of the present work. The assay buffer (1 mM Tricine, 50 mM KCl, 2 mM $MgCl_2$, NaOH to pH 8.0) was supplemented with 2 mM PEP, 2 mM ADP, 0.15 mM NADH, 25 U/ml LDH. The reaction was started in the spectrophotometer by addition of a suitable volume of PK solution, and the ensuing NADH oxidation, stoichiometrically coupled to ADP phosphorylation, was recorded at 340 nm as a function of time. By carrying out the same measurements as a function of [ADP], an hyperbolic course was obtained, giving a K_M^{ADP} value of 0.15 mM. The ADP concentrations maintained at the different PK activities could be calculated by imposing that a steady state concentration for ADP is reached, in which the rate of its production by the ATP hydrolysis reaction ($v_{(hyd)}$) balances the rate of its depletion by PK ($v_{(PK)}$). Assuming a Michaelis–Menten kinetics for the PK reaction, one has:

$$v_{(hyd)} = v_{(PK)} = \frac{V_{max}^{ADP} \cdot [ADP]_{ss}}{[ADP]_{ss} + K_M^{ADP}} \quad (1)$$

where $[ADP]_{ss}$ is the ADP concentration in the steady state, and V_{max}^{ADP} and K_M^{ADP} refer to the PK reaction. V_{max}^{ADP} and K_M^{ADP} were measured as described above, and $v_{(hyd)}$ were those reported in Fig. 5E. Control measurements gave a K_i for ATP as a competitive inhibitor with ADP in the order of 2 mM, indicating that at the relatively low ATP concentrations of these assays (150 μM) the expected apparent K_M^{ADP} does not differ significantly from the K_M^{ADP}.

3. Results

To evaluate the extent of intrinsic uncoupling in the *E. coli* ATP synthase, we have purified the enzyme and reconstituted it into preformed liposomes, as described in Materials and methods. The activity of the purified enzyme and its substantial incorporation into the liposomes were assayed by measuring the rate of ATP synthesis driven by acid–base transitions (see below). Acid–base transitions were also applied with the aim of calibrating the response of the transmembrane ΔpH fluorescent probe ACMA, needed for a quantitative evaluation of proton pumping. A fundamental condition required in order to apply reliably a calibration obtained by acid–base transitions to the signals elicited by the EF_0F_1 proton pumping is that the percentage of vesicles devoid of pumps is close to zero, since they will respond to the imposed ΔpH but will not contribute to a signal due to proton pumping coupled to ATP hydrolysis. Therefore, the initial measurements were devoted to such goal.

3.1. ACMA quenching and catalytic activities of proteoliposomes as a function of EF_0F_1-to-lipid ratio

The method used for liposomes formation and EF_0F_1 reconstitution has been already described in [31]. The average diameter of the proteoliposomes resulting from such a procedure was 160 nm, as measured by Photon Correlation Spectroscopy [38,39]. Therefore, by taking an area of 0.64 nm^2/lipid molecule [40] and an average molecular weight of 780 Da for a lipid molecule, at a lipid concentration of 0.08 g/l, a proteoliposome concentration of 0.4 nM in the assays can be calculated. On the basis of the Bradford protein assay method and of a molecular weight of 530 kDa, the EF_0F_1 concentration in the assays, and therefore the average enzyme-to-vesicle ratio, can also be calculated. Assuming a Poisson distribution, the probability $P(x, n)$ of finding a given number of EF_0F_1 molecules

per vesicle (x) can be predicted for different values of the average number of EF_0F_1 molecules per vesicle (n), according to:

$$P(x,n) = \frac{n^x}{x!}e^{-n} \quad (2)$$

From such equation it results that the probability of having liposomes completely devoid of EF_0F_1s, for an average of 1, 2, 3, and 4 EF_0F_1 per vesicle, is 37%, 14%, 5%, and 2%, respectively. Therefore, in order to reduce such probability down to acceptable values, theory predicts that the EF_0F_1 concentration in the assays must exceed 1.2–1.6 nM.

To check for agreement with experimental data, a series of reconstitutions was set up, in which the EF_0F_1-to-vesicle ratio was varied by changing the amount of added protein. As expected, the hydrolysis rate (Fig. 1A) increased linearly with the enzyme concentration. The synthesis rate (Fig. 1B) also increased linearly with the enzyme concentration, indicating that the percentage of enzyme incorporated into the membrane was constant in the tested concentration range. The slopes of the plots in Fig. 1A and B give directly the turnover numbers in the hydrolysis ($19 \pm 2\ s^{-1}$) and synthesis ($63 \pm 3\ s^{-1}$) direction, respectively. Fig. 1C shows the ACMA fluorescence traces obtained from these different samples when the hydrolysis reaction was started, at $t = 0$, by adding ATP to the assay. Both the initial rate of quenching and the steady state quenching extent increased as a function of the enzyme-to-lipid ratio. If the size of the internal volume, V_{in}, in which the probe concentrates, is constant, a roughly linear increase of the initial quenching rate with the enzyme concentration is expected: in fact, (a) at low values the quenching is found to increase linearly with the ΔpH (see Fig. 2C below), i.e. with pH_{in} at constant pH_{out}, (b) at low values the $d(pH_{in})/dt$ is proportional to the acidification rate $d[H^+]_{in}/dt$, and (c) this latter rate is proportional to the number of pumped protons (see Eq. (6) below), i.e. to the number of incorporated enzyme molecules. In contrast, the initial quenching rates should increase with an upward concavity if not only the enzyme concentration but also the internal volume is increasing. The plot of the initial rates of quenching as a function of enzyme concentration is shown in Fig. 1D, and it is consistent with an upward concavity up to 1.5–2 nM enzyme (i.e. up to

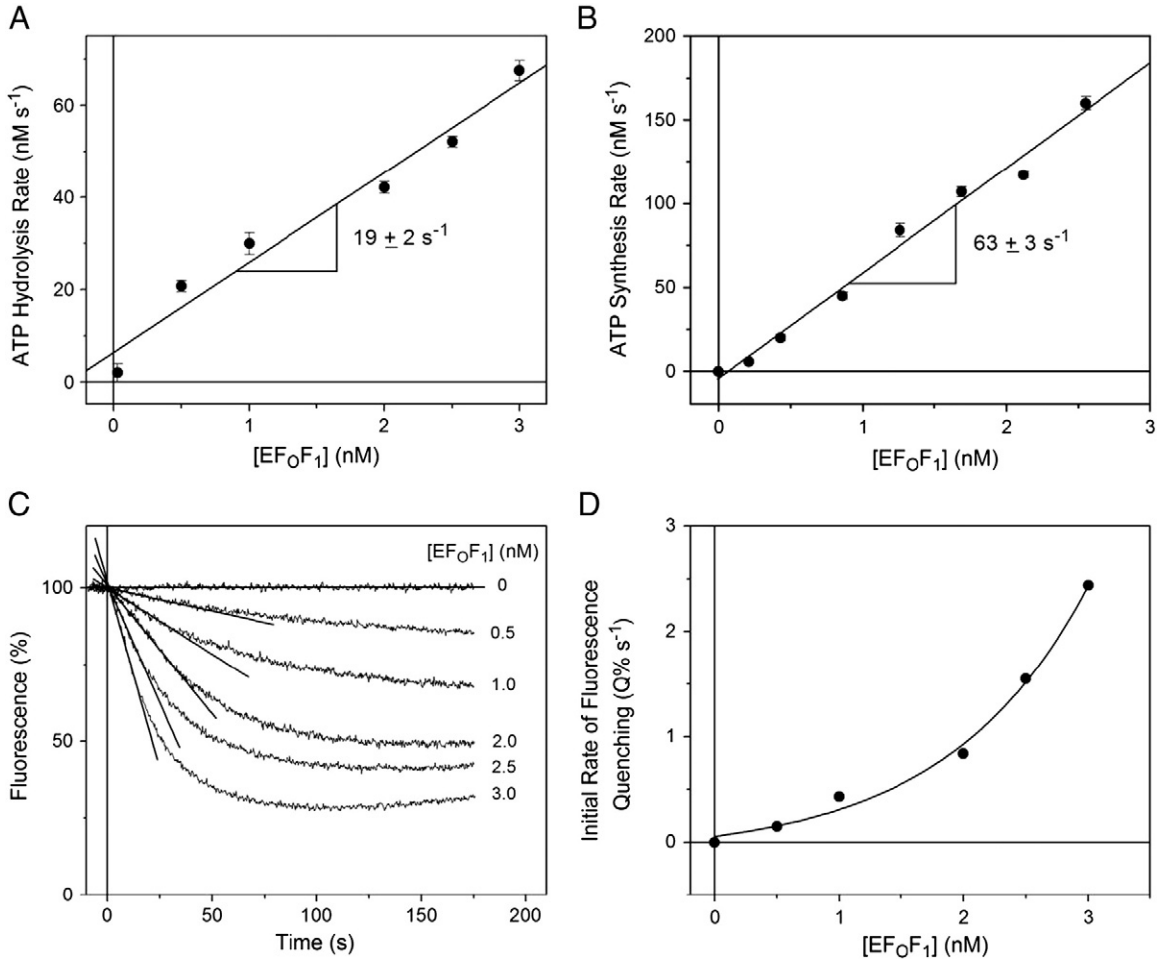

Fig. 1. ACMA quenching and catalytic activities in proteoliposomes as a function of EF_0F_1-to-lipid ratio. After reconstitution in the presence of increasing concentrations of EF_0F_1, the suspension was diluted in the measuring buffer, as described in Materials and methods. (A) The rates of ATP hydrolysis are plotted as a function of EF_0F_1 concentration. The ATP hydrolysis as a function of time, started by addition of 50 μM ATP and measured with the Phenol Red assay as described in Materials and methods, was linear over the whole recorded time range (not shown). The slopes and their standard deviations were calculated by linear regression fitting. The straight line in the plot is the linear regression fit of the data (slope = $19 \pm 2\ s^{-1}$). (B) The initial rates of ATP synthesis are plotted as a function of EF_0F_1 concentration. The ATP synthesis reaction was induced by an acid–base transition into the luminometer cuvette in the presence of the reaction substrates and ATP formation was monitored continuously in the luciferin/luciferase assay as described in Materials and methods. It decayed exponentially with a half-life of a few seconds (not shown). The initial rates and their standard deviation were calculated by linear regression fitting over the first second of reaction. The straight line in the plot is the linear regression fit of the data (slope = $63 \pm 3\ s^{-1}$). (C) The proton pumping reaction was started in the spectrofluorimeter cuvette by addition of 50 μM ATP at $t = 0$, and the ACMA fluorescence was recorded as a function of time. For each trace, addition of 1 μM nigericin recovered the 100% fluorescence level (not shown). The EF_0F_1 concentration in each assay is indicated. The straight lines, whose slopes represent the initial rates of quenching, were obtained by linear regression of the first few seconds of reaction. (D) The initial rates of quenching from (C) are plotted as a function of EF_0F_1 concentration. The standard deviations associated to the slopes were smaller than the size of the circles. The curve through the points is an arbitrary exponential function drawn to guide the eye.

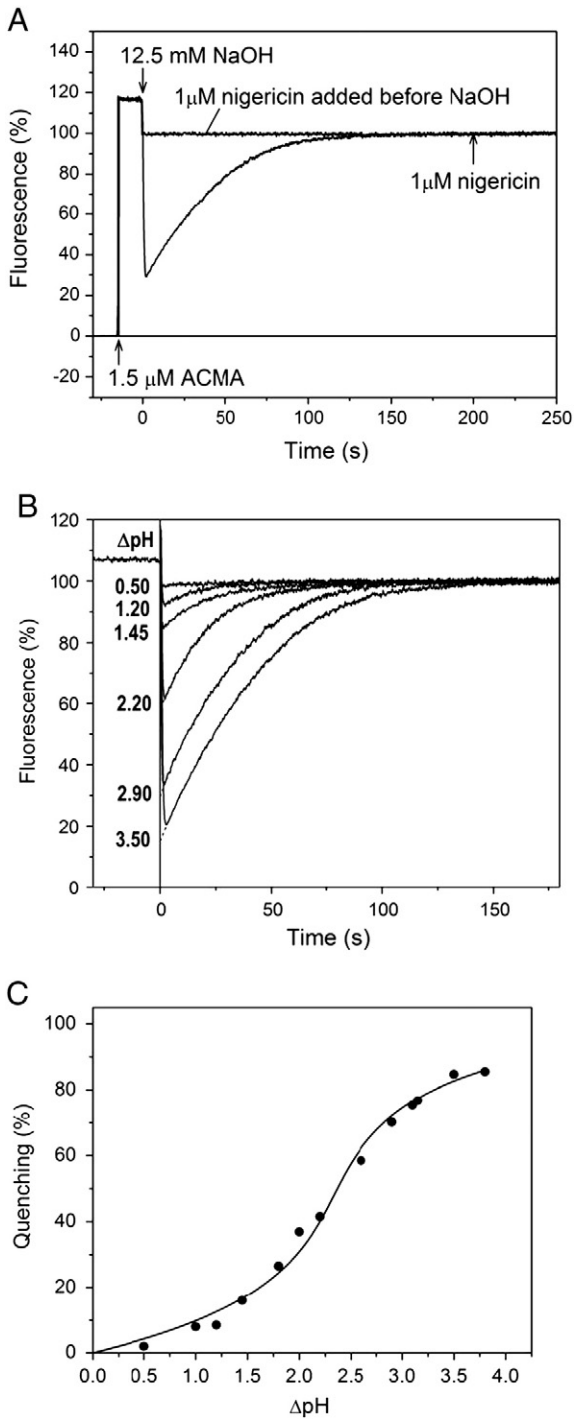

Fig. 2. Calibration of ACMA fluorescence quenching by acid–base transitions. (A) Where indicated, ACMA was added in the spectrofluorometer cuvette to the acidified proteoliposomes, which had a pH value of 5.1. The subsequent addition of NaOH to the indicated concentration brought rapidly the external pH to 8.0 and induced the transmembrane ΔpH transition. Nigericin added after the quenching transient was decayed did not change the fluorescence extent. Nigericin added prior to NaOH abolished the quenching transient. (B) Several acid–base transitions were induced at the different indicated ΔpH values, by addition of suited amounts of NaOH at time $t=0$. The fluorescence signal recorded prior to NaOH addition is shown for clarity only for the trace at ΔpH = 0.5. The dashed lines indicate the linear extrapolation to $t=0$ of the decaying traces. (C) The ACMA quenching values, extrapolated to $t=0$, as a function of ΔpH are from (B) and additional measurements. The line through the data points is the best fitting of Eq. (4) to the data. The values of the best fitting parameters were $A=19.2$, $B=149$, $C=-0.038$.

estimated 3.5–5 EF_0F_1 per vesicle) and a linear increase at higher values, in fair agreement with theory. As a whole, the experiments reported in Fig. 1 show that the enzyme reconstituted into liposomes behaved as it would be expected given a random distribution and proper insertion into the lipid bilayer. Routinely, a concentration of 3 nM enzyme was used in all subsequent experiments. This amount corresponds to an average number of about 7 enzymes per vesicle, and to a probability of completely empty liposome inferior to 0.1 %.

The relatively high rates of ATP synthesis indicate that the enzyme was well incorporated into liposomes. Such rates compare well with those reported in [32,41], which were obtained using the same reconstitution method and similar enzyme preparation procedures. In [41], a ratio of synthesis to hydrolysis rates of about 1 was obtained, with hydrolysis rates measured in an ATP regenerating system. A similar ratio was also found in our preparations when the rate of hydrolysis at saturating ATP concentration (and not at 50 μM) is considered (see below, Fig. 4).

3.2. Calibration of the ACMA response in proteoliposomes

Fluorescent amines have been largely used to detect a transmembrane ΔpH in natural and artificial membrane systems in which direct measurements are generally precluded by the small dimensions of the inner osmotic volume. A model for interpreting energy-dependent fluorescence changes was originally proposed by Schuldiner and coworkers [42]. This model assumes that amines behave ideally, are freely permeable through the membrane phase in their neutral form and re-distribute between the inner and outer aqueous compartments following the protonation–deprotonation equilibria which occur upon the generation of a transmembrane ΔpH (acidic inside). In the case of fluorescent amines, this equilibrium re-distribution is associated with a quenching of their fluorescence (Q) which, according to the model, would be promoted by accumulation of the probe in the inner aqueous compartment. This notion is consistent with the observation that the fluorescence is restored to its original level when the transmembrane ΔpH is dissipated by effectors such as uncoupling agents, ionophores and specific inhibitors of proton pumping. Therefore, based on these assumptions, for monoamine of high pK_a (pK_a » pH_{in}, pH_{out}), ΔpH is determined as:

$$\Delta pH_{out-in} = \mathrm{Log}\left(\frac{C_{in}}{C_{out}}\right) = Log\left(\frac{Q}{100-Q}\right) + \mathrm{Log}\left(\frac{V_{out}}{V_{in}}\right) \quad (3)$$

where C_{in} and C_{out} are the concentrations of the amine in the volumes of the inner (V_{in}) and outer (V_{out}) aqueous compartments, respectively, and Q is the percentage quenching of fluorescence.

After the above model had been tested for some time, it became clear that the probe behaves non-ideally in vesicle systems, in particular the empirical V_{in}/V_{out} values which were extrapolated from the experimental data turned out unreasonably high. The model by [42] has been modified by Casadio [43], who focused on the highly lipophilic probe ACMA. By taking into account the partition of ACMA into the lipid phase and the differential partition equilibria at the inner and outer vesicle faces, this modified model arrived at the following relationship between ΔpH and percentage fluorescence quenching (Q):

$$\Delta pH = A \cdot \frac{Q}{B-Q} e^{\left(\frac{Q}{B-Q} + C \cdot Q\right)} \quad (4)$$

where the three constants A, B and C are functions of various physical parameters, among which the adsorbing surfaces of the outer and inner membranes, and those defining the adsorption isotherm of the amine.

In the present work, our approach to evaluate the ΔpH in terms of percentage fluorescence quenching has been to measure the response

of ACMA elicited by a series of acid–base transitions imposed to the proteoliposomes, and then fit Eq. (4) to the data set of the measured ΔpH and Q values by finding the best-fitting values of the A, B, and C parameters.

In Fig. 2A, the fluorescence ACMA trace obtained upon one such transitions is shown. The ACMA was added, as indicated, to a liposome suspension previously acidified to pH 5.1 by addition of 12.5 mM HCl, and preincubated for 30 min to allow full equilibration between the external and the intravesicular aqueous compartments. Upon addition of 12.5 mM NaOH to rapidly bring the outside pH to 8.0, a transient ΔpH was established across the proteoliposome membrane, which was bound to decay due to the membrane permeability to protons. Correspondingly, a maximal fluorescence quenching was observed upon NaOH addition, which decayed within about 150 s. Addition of 1 μM nigericin at this point in time had no effect on ACMA fluorescence. The difference between the fluorescence value after complete ΔpH decay and the fluorescence value prior to NaOH addition can be ascribed to the different quantum yield of ACMA at different pH values. In fact, addition of nigericin prior to NaOH, which in the presence of valinomycin and KCl should collapse the imposed transmembrane ΔpH within few milliseconds, prevented the transient quenching of fluorescence, but resulted in the same difference of fluorescence values. Therefore, the 100% fluorescence intensity, to which the quenching was referred, was taken to be the signal recorded at pH 8.0 (i.e. after NaOH addition) after complete ΔpH equilibration had taken place.

Fig. 2B shows a collection of traces obtained at different ΔpH values, i.e. preincubated at different HCl concentrations. Each trace was linearly extrapolated to time $t=0$ and the extrapolated value was taken as the maximum extent of quenching induced by the imposed ΔpH. As expected, increasing quenching values were observed for increasing ΔpH values. In Fig. 2C, the maximum quenching values from Fig. 2B and from other measurements were plotted as a function of the imposed ΔpH value. This set of data constitutes a calibration of the ACMA response to the transmembrane ΔpH. It shows a sigmoidal trend, as predicted by Eq. (4). The line through the points is the result of a best fitting procedure of Eq. (4) to the data, in which the three parameters A, B and C were let free to fluctuate. This best-fitting function was utilized for converting the quenching data, resulting from ATP hydrolysis-coupled proton pumping, into the corresponding values of pH_{in}.

3.3. Effect of P_i on ATP hydrolysis and proton pumping

The ACMA calibration presented in the previous paragraph offered the possibility to analyze in a quantitative way the ACMA signals obtained by ATP hydrolysis-induced proton pumping in proteoliposomes. In particular, our aim was to analyze quantitatively the phenomenon of P_i- and ADP-induced modulation of proton pumping efficiency, which we have previously observed in the ATP synthase of *E. coli* [28] and of *Rb. capsulatus* [27] inverted membranes.

Inorganic phosphate monotonically inhibited the ATP hydrolysis of ATP synthase in *E. coli* membranes with an apparent K_d of 150 μM [28]. Therefore, we first measured ATP hydrolysis as a function of P_i, to check whether this trend could be reproduced in our isolated, reconstituted EF_0F_1. Fig. 3A shows the amount of hydrolyzed ATP as a function of time after addition of 50 μM ATP at $t=0$, as evaluated spectrophotometrically by the Phenol Red assay, in the presence of increasing P_i concentrations; valinomycin and 50 mM K^+ were also present, to keep the same conditions as in the ACMA assay (see below). The hydrolysis rates, which were largely constant over the measured time range, decreased by increasing P_i concentrations. After incubating the samples for 1 h in the presence of 250 μM DCCD, no activity was detectable (data not shown). By plotting the rates from Fig. 3A as a function of P_i, a hyperbolic trend was obtained (see below, Fig. 3F, full circles), with a half-maximal effect at $[P_i]=510\pm140$ μM. The linearity of the ATP hydrolysis traces as a function of time up to at least 150 s may appear somewhat surprising, given that during the same time interval a substantial transmembrane proton gradient has been building up for most, if not all, of the assays (see below, Fig. 3B, C). This proton gradient should in principle exert a backpressure on the proton-pumping ATP synthases, thus inhibiting their rates, and given that, e.g. for the control, 8–9 μM ADP have been produced in the assay at the end of 150 s. However, the F_OF_1 from *E. coli* has been shown to increase its potential rate of ATP hydrolysis as a function of increasing protonmotive force [44] (a rate measurable only transitorily immediately after dissipation of the proton gradient by e.g. uncouplers), similar in this regulatory behavior to what has been seen in the F_OF_1 from several other sources (see for a review [45]). Therefore, it is conceivable that such linearity resulted from a fine balance involving both an inhibition exerted by the protonmotive force backpressure (and by ADP) and a simultaneous stimulation by that very same protonmotive force. The ATP hydrolysis rate of F_OF_1 from *Rb. capsulatus* has indeed been shown to progress almost linearly for several minutes, while however activating itself up to about 6-fold due to the protonmotive force [46].

The proton translocating activity as a function of P_i was estimated in the ACMA assay under the same experimental conditions. The ionophore valinomycin and 50 mM K^+ were present in order to suppress the electrical component of the protonmotive force. Fig. 3B shows the ACMA fluorescence as a function of time in the presence of increasing P_i concentrations. The proton transport reaction was started by addition of 50 μM ATP at $t=0$, to which a fluorescence quenching followed in all cases, which could be reversed by addition of nigericin (not shown), indicating acidification of the vesicles interior. In contrast to the monotonic inhibitory trend observed for hydrolysis, increasing amounts of added P_i, up to 200 μM, induced an increase both of the initial rate and of the average steady state value of ACMA fluorescence quenching. An inhibitory effect, especially on the initial rate, was observed only at higher P_i concentrations, up to 3 mM. No significant fluorescence signal was detected in samples which had been preincubated for 1 h with 250 μM DCCD (not shown). It is interesting to note that, only in the absence of added P_i, a slow decrease of quenching settled in after 30–50 s, indicating an inhibition of proton pumping, which is at remarkable variance both with the linear course of the ATP hydrolysis in the same time range, and with the lower values of hydrolysis rates observed for the P_i containing samples (Fig. 3A).

Based on the calibration results presented in Fig. 2C, the quenching values were converted into internal $[H^+]$ values (Fig. 3C). This quantitative treatment of the fluorescence data offers a visual picture of the real time dependence of internal acidification, not distorted and flattened by the logarithmic definition of pH and by the non-linear response of ACMA fluorescence quenching to ΔpH. In such a linear plot, it is particularly evident that the presence of P_i led to a significant increase, over the 200 s of recording, of the internal acidification at almost all concentrations. In the absence of added P_i, after about 60 s of reaction, a progressive decrease of proton pumping could be observed whereas the ATP hydrolysis rate was unchanged. At its maximum value the internal proton concentration was about 8 μM, corresponding to a $\Delta pH=2.9$ units. Additions of 100 or 200 μM P_i prolonged the internal acidification up to the significant higher values of 54 μM ($\Delta pH=3.7$ units). If analyzed at longer reaction times, i.e. at lower internal pH's, the stimulation by P_i on proton pumping is, therefore, markedly higher than that shown in Fig. 3F. However, the data cannot be treated with comparable accuracy, since the outward flow cannot be ignored any more.

For a quantitative comparison of the ratios between internal acidification and ATP hydrolysis, we looked at the initial stages of the reaction (Fig. 3D), where the passive outward proton efflux J_{out} can still be considered negligible, since it depends on the internal acidification:

$$J_{out} = P_{H^+} \cdot \left(\left[H^+\right]_{in} - \left[H^+\right]_{out} \right) \quad (5)$$

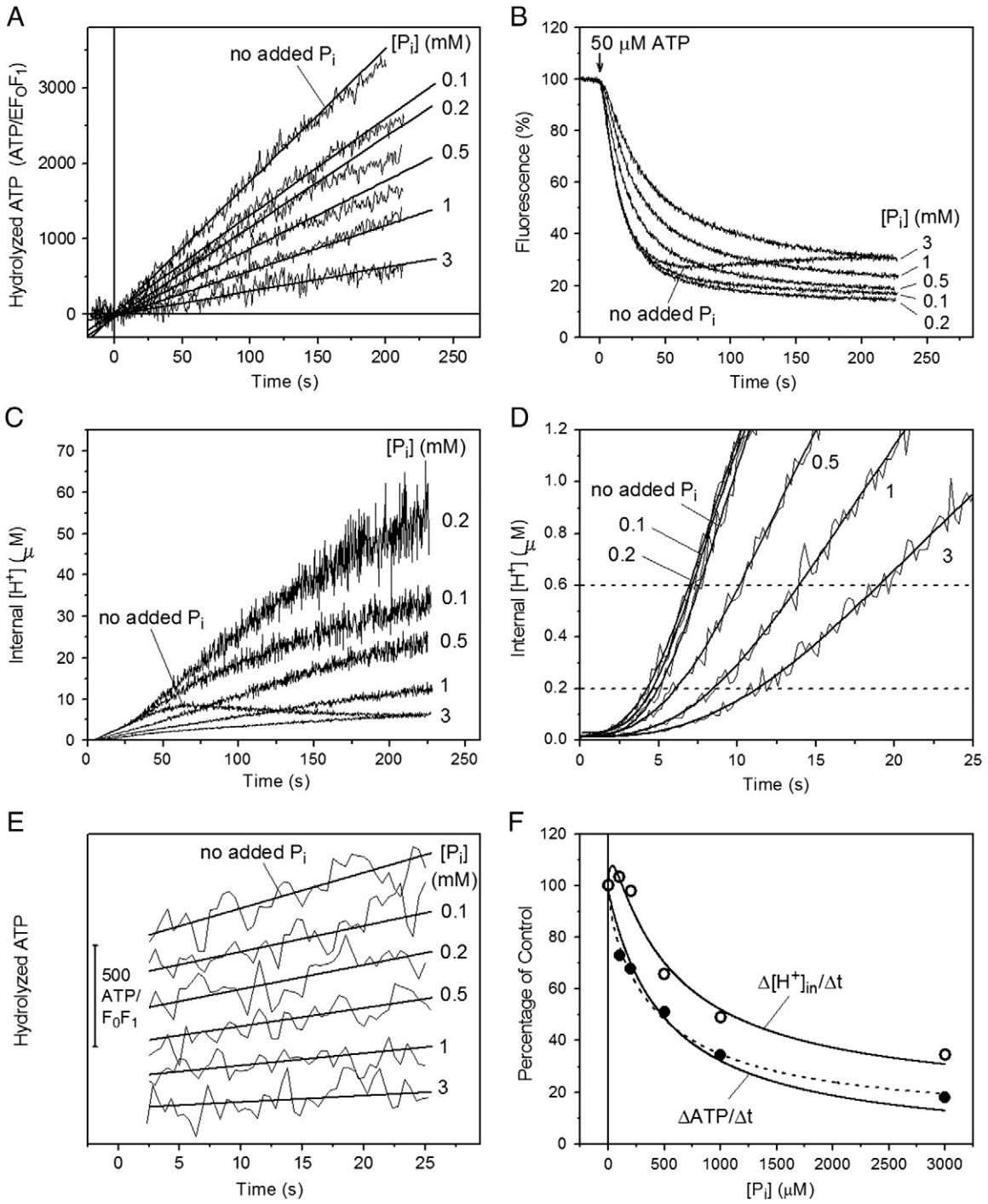

Fig. 3. ATP hydrolysis and proton pumping as a function of P_i concentration. (A) The ATP hydrolysis as a function of time was monitored spectrophotometrically by the Phenol Red assay as described in Materials and methods. For each P_i concentration, 50 μM ATP were added in the cuvette at time $t = 0$ to start the reaction, and the absorbance (625–587 nm) was measured as a function of time. Absorbance values were converted to hydrolyzed ATP as described in Materials and methods. Different P_i concentrations were added to each assay as indicated. The experimental traces were best fitted by linear functions up to 100 s. (B) The ACMA assay was carried out as described in Materials and methods. The proton pumping reaction was started in the spectrofluorometer cuvette by addition of 50 μM ATP at time $t = 0$ and the ACMA fluorescence was recorded as a function of time. Different P_i concentrations were added to each assay as indicated. (C) The traces from (B) are reported here after converting the percentage quenching values into internal $[H^+]$ values, based on the calibration function from Fig. 2C. (D) The traces from (C) are reported on a shorter time scale, showing the initial stages of the reaction. The numbers are P_i concentrations in mM units. To improve precision in reading the times values corresponding to $[H^+]_{in} = 0.2$ and $[H^+]_{in} = 0.6$ μM, the traces have been fitted by arbitrary sigmoidal functions (continuous lines). (E) The traces and fitting straight lines from (A) are reported on a shorter time scale, showing the initial stages of the reaction. (F) Percentage values, relative to the value in the absence of added P_i ("control"), of the average ATP hydrolysis rates, $\Delta ATP/\Delta t$ (●, from (E)) and of the average rates of internal acidification, $\Delta[H^+]_{in}/\Delta t$ (**O**, from (D)). Control values were 17.6 s^{-1} for $\Delta ATP/\Delta t$ and 0.15 μM·s^{-1} for $\Delta[H^+]_{in}/\Delta t$. The curve (continuous line) through the average ATP hydrolysis data points is the best fit to the data of the hyperbolic function $P_1 - P_2 \cdot x/(P_3 + x)$, with resulting best fit parameter $P_3 = 510$ μM ± 140 μM, corresponding to the apparent K_d value. The dashed line is the function $P_1 - P_2 \cdot x/(P_3 + x) - P_4 \cdot x/(P_5 + x)$, with imposed parameters $P_3 = 30$ μM and $P_5 = 510$ μM. The curve through the $\Delta[H^+]_{in}/\Delta t$ data points is the best fit to the data of the double hyperbolic function $P_1 + P_2 \cdot x/(P_3 + x) - P_4 \cdot x/(P_5 + x)$ with imposed parameters $P_3 = 30$ μM and $P_5 = 510$ μM. These values were imposed due to the high uncertainties associated to the high number of floating parameters relative to the number of data points.

(where P_{H^+} is the H^+-permeability coefficient of the proteoliposome membrane). In the absence of passive proton efflux, the rate of internal acidification can be written as:

$$d\left[H^+\right]_{in}/dt = \left(V_{in}\cdot \boldsymbol{B}\left(\left[H^+\right]_{in}\right)\right)^{-1}\cdot dn_{H^+}/dt = \left(\boldsymbol{B}\left(\left[H^+\right]_{in}\right)\right)^{-1} \cdot R_{H+/ATP}\cdot E/(N_A\cdot V_{in})\cdot dATP/dt \quad (6)$$

where $\boldsymbol{B}([H^+]_{in})$ is a function of the buffer capacity of the internal compartment, (see Appendix), dn_{H^+}/dt is the number of proton moles translocated to the inner compartment in the time unit, $R_{H+/ATP}$ is the ratio of proton translocated per hydrolyzed ATP, E is the average number of ATP synthase per vesicle, N_A is the Avogadro number, V_{in} is the vesicle inner volume and $dATP/dt$ is the rate of ATP hydrolysis per F_0F_1. The parameter $\boldsymbol{B}([H^+]_{in})$ which entails the endogenous buffering components of the vesicles and, to a minor degree, the exogenous buffers, is a single valued function of $[H^+]_{in}$, and can be simulated by a summation of a number of formal buffers whose protonation degree depends on their concentration and pK's (see Appendix). Therefore, the buffering capacity for each $[H^+]_{in}$ value can be assumed to be largely unchanged in our assays, performed under identical conditions, irrespective of the different P_i concentration, since this anion should not permeate the lipid bilayer. Even if some permeation of P_i through the membrane should have occurred during the 15 min of liposome incubation in the measuring buffer prior to the start of the reaction (which is unlikely, given its 1–2 negative charges at pH 8), the internal buffer capacity would have increased as a function of P_i, and therefore it could not explain the observed increase in the rate of acidification at P_i<200 μM (see below).

Ideally, Eq. (6) holds only at the very start of the reaction, when the difference $([H^+]_{in}-[H^+]_{out})$, and thus the passive proton flux (Eq. (5)), is zero. Due to the experimental uncertainties of the signals at $t=0$ s, characterized by a low signal-to-noise ratio both in the ACMA and Phenol Red assays, and by dilution and mixing artifacts, our data did not allow a reliable determination of the initial rates. However, to our purpose of a comparison between the different P_i concentrations, the passive outward flux induced by the $([H^+]_{in}-[H^+]_{out})$ difference could be considered negligible–relative to the active inward proton flux–also a few seconds after the reaction start, up to $([H^+]_{in}-[H^+]_{out})$ values which do not exceed 5–10% of the maximal ones. In fact, for $([H^+]_{in}-[H^+]_{out})$ values which are 1–2 orders of magnitude lower than at steady state (at which $J_{out}=J_{in}$), J_{out} has to be correspondingly lower (see Eq. (5)), while J_{in} should be practically the same if it is proportional to the hydrolysis rate (see Fig. 3A). In addition, instead of instantaneous rates, in order to improve precision in the determination of the ratios between internal acidification and ATP hydrolysis, we chose to use averaged rates:

$$\Delta\left[H^+\right]_{in}/\Delta t = \left(V_{in}\cdot \boldsymbol{B}\left(\left[H^+\right]_{in}\right)\right)^{-1}\cdot \Delta n_{H^+}/\Delta t = \left(\boldsymbol{B}\left(\left[H^+\right]_{in}\right)\right)^{-1} \cdot R_{H+/ATP}\cdot E/(N_A\cdot V_{in})\cdot \Delta ATP/\Delta t \quad (7)$$

Since the parameter $\boldsymbol{B}([H^+]_{in})$ was a function of $[H^+]_{in}$, we selected the same $\Delta[H^+]_{in}$ interval for all traces, namely 0.2–0.6 μM (pH_{in} 6.7 and 6.2 respectively), as indicated by the dashed lines in Fig. 3D. These two values satisfy the above conditions: $[H^+]_{in}=0.2$ μM is reached usually after at least 3÷5 s of hydrolysis, a time sufficient to dissipate any mixing artifact, and $[H^+]_{in}=0.6$ μM is sufficiently low for neglecting the outward flux as compared to the inward protons pumping. The number or protons pumped in the inner compartment under these conditions is measured quantitatively by $V_{in}\cdot\boldsymbol{B}([H^+]_{in})\cdot([H^+]_{final}-[H^+]_{initial})$, where $\boldsymbol{B}([H^+]_{in})$ is a quantity which is undetermined but constant for all experiments. For each trace, the corresponding Δt were read and used to determine the ΔATP per F_0F_1 hydrolyzed in that time interval (see Fig. 3E for an enlarged view of Fig. 3A). The resulting $\Delta[H^+]_{in}/\Delta t$ and $\Delta ATP/\Delta t$ values are plotted in Fig. 3F. All values have been expressed as percentages of the value measured in the absence of added P_i, such as to eliminate the undetermined quantities $(\boldsymbol{B}([H^+]_{in}))^{-1}\cdot E/V_{in}$. The plot shows that the averaged ATP hydrolysis rates (closed circles) decrease monotonically as a function of P_i concentration, whereas the averaged rates of acidification (open circles) show a parallel decrease only after a first phase of increase taking place up to about $[P_i]$<200 μM. Similar results were obtained in several other series of measurements carried out with different reconstitution batches. The $\Delta[H^+]_{in}/\Delta t$ data could be fitted by the sum of a rising hyperbolic function with imposed $K_d=30$ μM and a descending hyperbolic function, with imposed $K_d=510$ μM, whereas the ATP hydrolysis data could be fitted by a descending hyperbolic function, with $K_d=510$ μM. The hydrolysis data were also compatible with a fitting by the sum of two descending hyperbolic functions (dashed line, with imposed $K_d(1)=30$ μM and imposed $K_d(2)=510$ μM) but the experimental error was too large to discriminate between these two possibilities.

We conclude that the divergence between $\Delta[H^+]_{in}/\Delta t$ and $\Delta ATP/\Delta t$ in the range $[P_i]$<200 μM indicates that, in such range, the $R_{H+/ATP}$ increases as a function of P_i. In addition, the biphasic course of the $\Delta[H^+]_{in}/\Delta t$ as a function of P_i indicates that the enzyme can bind P_i at two different sites, one of which with an apparent K_d in the order of tens of micromolar, whose occupancy by P_i appears mainly to stimulate the proton pumping efficiency, and a second one with an apparent K_d in the order of hundreds of micromolar, whose occupancy by P_i appears mainly to inhibit ATP hydrolysis, and proton pumping in parallel.

3.4. ATP hydrolysis and proton pumping as a function of ATP concentration

To test the reliability of our system, we have measured ATP hydrolysis and proton pumping in parallel as a function of ATP concentration, i.e. under conditions which, as far as we know, should not result in a change of the coupling efficiency of the ATP synthase. Fig. 4A shows the ACMA fluorescence quenching as a function of time in the presence of increasing ATP concentrations. The proton transport reaction was started by addition of ATP at $t=0$. Both the initial quenching rates and the steady state quenching increased with increasing ATP. In Fig. 4B the fluorescence quenching values were converted into the corresponding $[H^+]_{in}$ values, according to the calibration of Fig. 2C, and plotted in an expanded scale, i.e. for concentration values below 1.2 μM. Similar to what was done for the dependency on P_i, an average acidification rate $\Delta[H^+]_{in}/\Delta t$ was evaluated over a fixed range of internal $[H^+]$ values, i.e. 0.2–0.6 μM (dashed lines in Fig 4B). For each trace, the corresponding Δt values were read and used to determine the ΔATP per F_0F_1 hydrolyzed in that time interval, taken from the ATP hydrolysis rates measured with the Phenol Red assay (not shown) which were constant over several tens of seconds. The resulting $\Delta[H^+]_{in}/\Delta t$ and $\Delta ATP/\Delta t$ values are plotted in Fig. 4C as a function of ATP concentration. Based on Eq. (7), these two sets of rates are predicted to be linearly related, provided $R_{H+/ATP}$ is constant. As evident in the figure, the two rates run in a closely parallel fashion up to approximately 100 μM ATP. The K_M value for ATP hydrolysis resulting from the fitting with a hyperbolic function (60 ± 4 μM) was lower than the reported value of 140 μM, obtained however in the isolated enzyme and under otherwise different experimental conditions [41]. The K_M value for ATP acidification resulting from the fitting with a hyperbolic function (35 ± 6 μM) was significantly lower, being influenced by the stronger saturation of the rates at higher ATP concentrations. This divergence between $\Delta[H^+]_{in}/\Delta t$ and $\Delta ATP/\Delta t$ values at the higher ATP concentrations can be due either to the fact that the accuracy of the calibration curve (Fig. 2C) is not constant over the entire ΔpH range, or to the fact that the $R_{H+/ATP}$ is not constant. In our opinion, neither of the two possibilities can be excluded, the former because the precision of the pH-meter is linear with the ΔpH, i.e. exponential with the proton concentration, and also because a larger error occurs at the higher ΔpH values in extrapolating to $t=0$ the

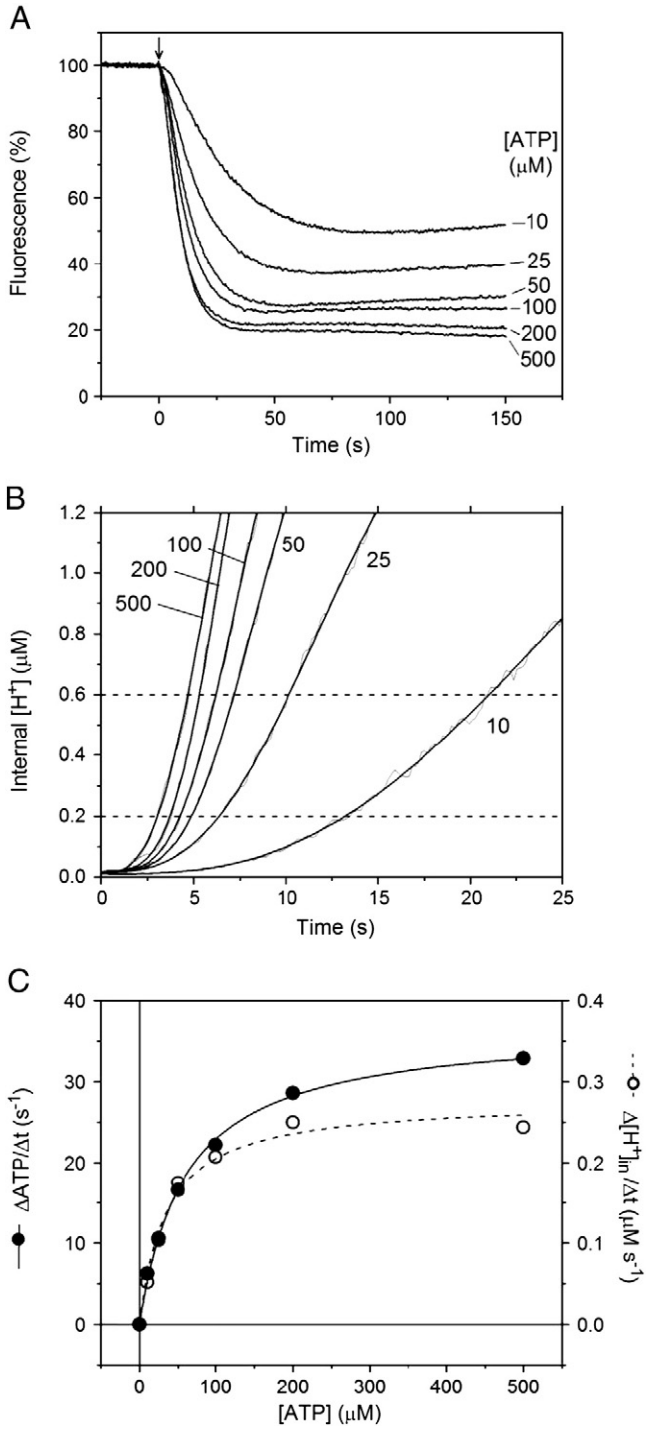

Fig. 4. ATP hydrolysis and proton pumping as a function of ATP concentration. (A) The ACMA assay was carried out as described in Materials and Methods. The proton pumping reaction was started in the spectrofluorometer cuvette by addition of different ATP concentrations (as indicated) at time $t = 0$ (arrow) and the ACMA fluorescence was recorded as a function of time. (B) The traces from (A) are reported here on a shorter time scale after converting the percentage quenching values into $[H^+]_{in}$ values, based on the calibration function from Fig. 2C. The numbers are ATP concentrations in μM units. To improve precision in reading the times values corresponding to $[H^+]_{in} = 0.2$ and $[H^+]_{in} = 0.6$ μM, the traces have been fitted by arbitrary sigmoidal functions (continuous lines). (C) The ATP hydrolysis average rates, $\Delta ATP/\Delta t$, as a function of ATP (●) were determined by linear fit of the original traces (not shown) measured spectrophotometrically by the Phenol Red assay as described in Materials and methods. The average rates of internal acidification, $\Delta[H^+]_{in}/\Delta t$ (**O**) are from (B). The curves through the data points are best fitting hyperbolic functions, with apparent K_M values of 61 ± 4 μM for $\Delta ATP/\Delta t$ (solid line), and 35 ± 6 μM for $\Delta[H^+]_{in}/\Delta t$ (dashed line).

decaying quenching registered after the acid–base transition, the latter because we cannot exclude that the ATP synthase efficiency decreases somewhat as a function of ATP concentration.

The data of Fig. 4C confirm that, under conditions which do not contemplate major changes in the coupling efficiency of the enzyme, the $\Delta[H^+]_{in}/\Delta t$ and $\Delta ATP/\Delta t$ have a parallel course at least up to approximately 100 μM ATP, and at the same time confirm the competence of our system to monitor the coupling degree up to relatively high rate values, both of ATP hydrolysis and of acidification, significantly higher than those measured under the conditions of Fig. 3.

3.5. Effect of ADP depletion on ATP hydrolysis and proton pumping

Both in *Rb. capsulatus* [27] and in *E. coli* inverted membranes [28], an increasing ADP depletion obtained by increasing amount of PK in the assays was shown to progressively reduce the proton pumping efficiency of the ATP synthase. We measured therefore in parallel both ATP hydrolysis and proton pumping in the proteoliposomes in the presence of increasing amounts of PK.

Except for the presence of PEP, the experimental conditions for the control (no added PK) were the same as those adopted for the control (no added P_i) in Fig. 3A and B. Fig. 5A shows ATP hydrolysis traces as a function of time in the presence of PEP and of increasing PK amounts. Under these conditions, the steady state ADP concentrations are predicted to progressively decrease in the series of assays (see Measurement of pyruvate kinase activity and evaluation of the steady state ADP concentration in the ADP rephosphorylation assay). The trace at 0 U/ml PK was obtained by the Phenol Red assay, while the traces in the presence of PK were obtained by the ADP rephosphorylation assay. The traces obtained at 25 and 50 U/ml PK were superimposable to the one at 10 U/ml PK, and are not shown for clarity. Similar to Fig. 3A, also in these series of measurements the hydrolysis rates were constant over the recorded time range. A significant increase in the rate could be observed at increasing PK amounts in the assay, up to 10 U/ml (see below, Fig. 5E, full circles).

The proton translocating activity as a function of PK was estimated in the ACMA assay under the same experimental conditions as used for the hydrolysis assay, except that ACMA was added and, in the PK-containing samples, LDH and NADH were omitted. Fig. 5B shows the ACMA fluorescence traces registered as a function of time in the presence of increasing PK amounts from 0 to 50 U/ml. The proton transport reaction was started by addition of 50 μM ATP at $t = 0$, to which a fluorescence quenching followed in each case, which could be reversed by addition of nigericin (not shown). Relative to the control in the absence of PK, addition of increasing amounts of PK induced first an increase of the average steady state value of ACMA fluorescence quenching (trace at 2.5 U/ml), but a decrease at higher values, in remarkable contrast to the overall increase observed in the corresponding hydrolysis rates. Though an initial increasing phase as a function of PK is not apparent if the initial rates of fluorescence quenching are considered, a significant decrease in those rates can be observed at higher PK values. Control measurements in which either the PEP or the PK were omitted or pyruvate up to 100 μM was added, did not differ significantly from the trace obtained at 0 PK, either in the initial rate of fluorescence quenching or in the quenching value at 100 s (not shown), indicating that these components per se did not affect the ATP synthase activity or the permeability of the phospholipid membrane.

In Fig. 5C the fluorescence traces were converted into internal $[H^+]$ values. As in Fig. 3C, the linear scale visually emphasizes the significant decrease in the internal acidification induced by increasing amounts of PK. Similarly to what was done for the dependency on P_i, an average acidification rate $\Delta[H^+]_{in}/\Delta t$ was evaluated over a fixed range of internal $[H^+]$ values, i.e. 0.2–0.6 μM (dashed lines in Fig 5D). For each trace, the corresponding Δt values were read and used to determine the ΔATP per F_0F_1 hydrolyzed in that time interval

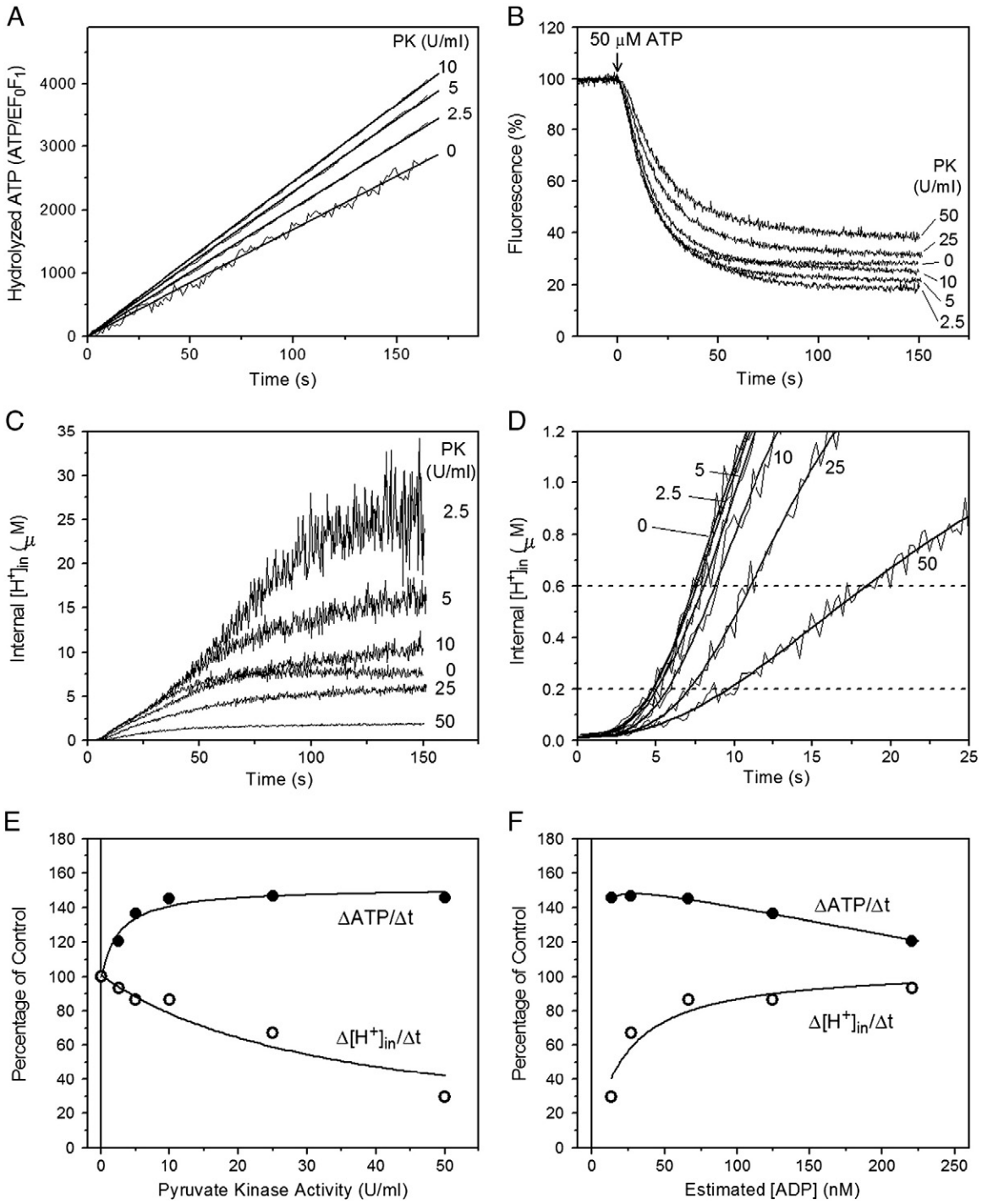

Fig. 5. ATP hydrolysis and proton pumping in the presence of increasing PK activity. (A) The ATP hydrolysis as a function of time was monitored spectrophotometrically by the Phenol Red assay (no added PK) or by the ADP rephosphorylation assay, as described in Materials and methods. For each PK activity, 50 μM ATP were added in the cuvette at time $t = 0$ to start the reaction, and the absorbance (625–587 nm for the Phenol Red assay, or 340 nm for the ADP rephosphorylation assay) was measured as a function of time. Absorbance values were converted to hydrolyzed ATP as described in Materials and Methods. Different PK activities were present in each assay as indicated. The traces obtained at 25 and 50 U/ml PK were superimposable to the one at 10 U/ml PK, and are not shown for clarity. The experimental traces were best fitted by linear functions up to 100 s. (B) The ACMA assay was carried out as described in Materials and methods, in the presence of 2 mM PEP and increasing amounts of PK as indicated. The proton pumping reaction was started by injecting 50 μM ATP at time $t = 0$ (arrow) in the spectrofluorometer cuvette, 15 min after addition of PK, and the ACMA fluorescence was recorded as a function of time. (C) The traces from (B) are reported here after converting the percentage quenching values into internal $[H^+]$ values, based on the calibration function from Fig. 2C. (D) The traces from (C) are reported on a shorter time scale, showing the initial stages of the reaction. The numbers are PK activities in U/ml. To improve precision in reading the times values corresponding to $[H^+]_{in} = 0.2$ and $[H^+]_{in} = 0.6$ μM, the traces have been fitted by arbitrary sigmoidal functions (continuous lines). (E) Percentage values, relative to the value in the absence of added PK ("control"), of the average ATP hydrolysis rates, $\Delta ATP/\Delta t$ (●, from (A) and additional measurements) and of the average rates of internal acidification, $\Delta[H^+]_{in}/\Delta t$ (**O**, from (D)). Control values were 16.9 s^{-1} for ATP hydrolysis rates and 0.15 μM·s^{-1} for $\Delta[H^+]_{in}/\Delta t$. The curves through the data points are best fitting single hyperbolic functions, drawn to guide the eye. (F) All rates values from (E), except for those in the absence of PK, which were omitted, are plotted here as a function of the estimated steady state ADP concentration, which was calculated for each PK concentration as described in Materials and methods (Measurement of pyruvate kinase activity and evaluation of the steady state ADP concentration in the ADP rephosphorylation assay). The curve through the $\Delta[H^+]_{in}/\Delta t$ data points is a fitting hyperbolic function, with a resulting apparent K_d of 21 ± 8 nM with imposed starting point at 0. The curves through the $\Delta ATP/\Delta t$ data points were the best fits to the data of double hyperbolic functions, drawn to guide the eye.

(Fig. 5A). The resulting $\Delta[H^+]_{in}/\Delta t$ and $\Delta ATP/\Delta t$ values are plotted in Fig. 5E. All values have been expressed as percentages of the value measured in the absence of added PK. The plot shows that the averaged ATP hydrolysis rates (closed circles) and the averaged rates of acidification (open circles) significantly diverge as a function of the added PK, since the first ones increase monotonically with the second ones showing a concomitant decrease. Similar results were obtained in several other series of measurements carried out with different reconstitution batches. As already noticed for the range of $[P_i]<$ 200 μM, this divergence between $\Delta[H^+]_{in}/\Delta t$ and $\Delta ATP/\Delta t$ indicates that the $R_{H+/ATP}$ decreases as a function of added PK.

The ADP concentrations at the different PK activities can be estimated by assuming that a steady state concentration for ADP is reached (as indicated by the observed constancy of the NADH oxidation rate, evidence for a constant pyruvate, i.e. ADP, concentration, in the assay), at which its rate of production by the ATP hydrolysis reaction ($v_{(hyd)}$) balances the rate of ADP depletion by the PK ($v_{(PK)}$), and considering a Michaelis-Menten kinetics of the PK reaction (see Eq. (1)). In Fig. 5F, the data from Fig. 5E have been reported as a function of the estimated steady state ADP concentrations. Here the lowest estimated ADP concentration (13 nM) corresponds to the highest PK activity (50 U/ml). The curve through the data points of the rate of $\Delta[H^+]_{in}/\Delta t$ is a fitting hyperbolic function, with a resulting apparent K_d of 16 ± 11 nM and a starting point close to 0. The rate of hydrolysis plotted in such a way appears to be unaffected by ADP up to about 70 nM, while an increasing inhibition can be observed at higher concentrations. On the contrary, most of the enhancing effect of ADP on $\Delta[H^+]_{in}/\Delta t$ is observed below 50 nM. Therefore, this set of data indicates the involvement of two ADP binding sites, with the highest affinity one affecting coupling, but not the hydrolysis rate, and the lower affinity one inhibiting the hydrolysis rate, but not affecting coupling. The affinity of the first site for ADP appears to be extremely high, especially in view of the fact that high and potentially competitive ATP concentrations (50 μM) are also present. In addition, the starting point close to 0 suggests that a total ADP release from that site will cause a total uncoupling. A biphasic response to ADP concentration is also evident when reaction times longer that 60 s are considered (Fig. 3C): a partial ADP depletion (PK = 2.5 U/ml) increases significantly the internal acidification relative to the control, consistent with an increased, and still substantially coupled, ATP hydrolysis, while higher PK amounts progressively suppress the extent of internal acidification, in spite of basically unaffected hydrolysis rates. Incidentally, this different response observed as a function of PK at times longer than 60 s, relative to the one observed at the initial stages of the reaction, where a monotonic inhibition of the internal acidification rate is measured, points to an involvement of the protonmotive force in modulating the degree of uncoupling. However, we have not further investigated this possibility.

3.6. Effect of ADP depletion on the P_i dependence of ATP hydrolysis and proton pumping

The P_i and ADP binding to the *E. coli* ATP synthase have been previously shown to act synergistically in the inhibition of ATP hydrolysis [28,44] and in the uncoupling effect [28]. In particular, the latter work [28] has shown that both the inhibitory and the coupling effects observed in inverted membranes as a function of P_i were lost if the medium ADP concentration was depleted by a sufficiently high amount of PK. Therefore, we repeated the measurements of Fig. 5, i.e. ATP hydrolysis and proton pumping in the presence of PK, but keeping the PK amount fixed at 25 U//ml PK, while the P_i concentration was varied. The resulting percentage values of $\Delta ATP/\Delta t$ and $\Delta[H^+]_{in}/\Delta t$ are collected in Fig. 6. Compared to the P_i-dependence obtained in the absence of PK (Fig. 3), the marked inhibition on the hydrolysis rates and on the internal acidification are largely lost, confirming also in the isolated and reconstituted EF_0F_1 that, in order for P_i to elicit its inhibitory and coupling effects, enzyme-bound ADP is required.

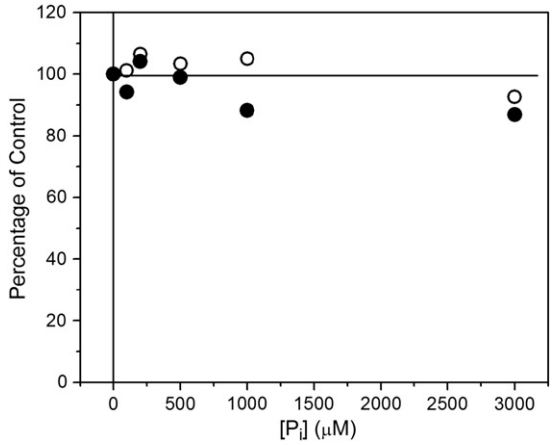

Fig. 6. ATP hydrolysis and proton pumping and as a function of P_i in the presence of 25 U/ml PK. All data are expressed as percentage relative to the values in the absence of P_i. The average ATP hydrolysis rates, $\Delta ATP/\Delta t$, (●) were determined by linear fit of the original traces (not shown) measured spectrophotometrically by the ADP rephosphorylation method as described in Materials and methods, in the presence of different amounts of P_i. The average rates of internal acidification, $\Delta[H^+]_{in}/\Delta t$ (**O**) were determined by converting the ACMA fluorescence traces recorded as a function of time (not shown) into $[H^+]_{in}$ values, based on the calibration function from Fig. 2C, and reading the times values corresponding to $[H^+]_{in} = 0.2$ and $[H^+]_{in} = 0.6$ μM. Control values were 24 s^{-1} for $\Delta ATP/\Delta t$, and 0.1 μM s^{-1} for $\Delta[H^+]_{in}/\Delta t$.

3.7. Quantitative evaluation of the relative uncoupling induced by P_i and ADP depletion

By making the conversion from ACMA fluorescence quenching values to ΔpH values possible, the ACMA calibration (Fig. 2) allows a quantitative evaluation of the uncoupling degree. According to Eq. (7), the ratio of the acidification rate $\Delta[H^+]_{in}/\Delta t$ to the hydrolysis rate $\Delta ATP/\Delta t$ (in s^{-1}) is equivalent to $(\boldsymbol{B}([H^+]_{in}))^{-1} \cdot R_{H+/ATP} \cdot E/(N_A \cdot V_{in})$. If $R_{H+/ATP}$ is not constant, its relative change can be obtained from such ratio, since all other parameters ($\boldsymbol{B}([H^+]_{in})$, E, N_A, V_{in}) were constant under our conditions. In Fig 7A, the $(\Delta[H^+]_{in}/\Delta t)/(\Delta ATP/\Delta t)$ ratios (values from Fig. 3F) were plotted as a function of P_i concentration. Analogously, Fig. 7B collects the $(\Delta[H^+]_{in}/\Delta t)/(\Delta ATP/\Delta t)$ ratios (values from Fig. 5F) as a function of the estimated ADP concentration. The best-fitting hyperbole in Fig. 7A indicates an increase of $R_{H+/ATP}$ up to 1.7-fold at saturating P_i concentrations, with an apparent K_d value of 220 ± 160 μM. The data points of Fig. 7B indicate a decrease of $R_{H+/ATP}$, relative to the control in the absence of PK, down to about 0.2-fold at the highest added PK amount, i.e. at the minimum ADP concentration reached. When referred to the 1.7 higher coupling ratio which, according to Fig. 7A, can be reached at saturating P_i, this maximum decrease corresponds to about 0.1-fold. The best-fitting hyperbole was obtained by imposing that it starts from 0, which is equivalent to assuming that the pump can be totally uncoupled when the site is fully emptied, and its apparent K_d has a value of 27 ± 9 nM. On the other hand, if the start value was let free to float, the corresponding best-fit values were 0.27 for the start, and 114 nM for the apparent K_d. The χ^2 of the two fittings was comparable, however the hypothesis of a totally uncoupled state appears to us more likely.

4. Discussion

In the present work the phenomenon of intrinsic uncoupling, previously described for the ATP synthases of *Rb. capsulatus* [27] and *E. coli* [28] in inverted native membranes, has been further investigated in the isolated and reconstituted enzyme from the latter organism. Similarly as found in inverted membranes, in the isolated

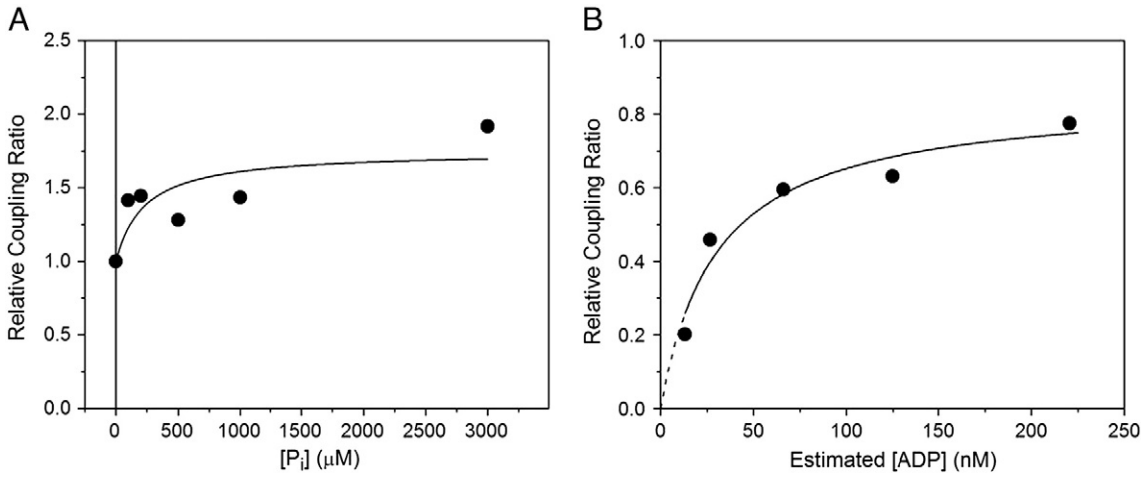

Fig. 7. Quantitative evaluation of the uncoupling degree induced by P_i and ADP depletion. (A) The ratios between the average rates of internal acidification, $\Delta[H^+]_{in}/\Delta t$, and the average rates of ATP hydrolysis, $\Delta ATP/\Delta t$, are reported as a function of P_i. Both sets of data were taken as percentage values relative to their control in the absence of P_i, and are from Fig. 3F. The best-fitting hyperbole has an apparent K_d value of 220 ± 160 μM. (B) The ratios between the average rates of internal acidification, $\Delta[H^+]_{in}/\Delta t$, and the average rates of ATP hydrolysis, $\Delta ATP/\Delta t$, are reported as a function of the estimated ADP concentration during steady state. Both sets of data were taken as percentage values relative to their control in the absence of PK, and are from Fig. 5F. The best-fitting hyperbole has an apparent K_d value of 27 ± 9 nM and an intercept at the *y*-axis imposed equal to 0.

and reconstituted EF_0F_1 the pumping efficiency has proven to be variable, and to be under the influence of ADP and P_i. The proteoliposome system, contrary to the inverted membrane system, has allowed us to obtain a calibration of the ΔpH-sensitive ACMA fluorescence quenching by means of acid–base transitions, making it possible to quantitatively estimate the relative changes in the coupling ratio of the pump as a function of ADP and P_i concentration.

The very low passive proton permeability of the proteoliposome system we have used has turned out to be well suited for evaluation of the ACMA quenching signal elicited by acid–base transitions carried out by manual mixing. The calibration curve had a sigmoidal course (Fig. 2C), consistent with previous experimental calibration curves obtained both with ACMA and 9-aminoacridine in inverted membranes of *Rb. capsulatus* [37,43], and with the theoretical model proposed in [43], which takes into account not only the protonic dissociation equilibria of the amine, but also the absorption of the highly lipophilic probe into the membrane phase and its partition equilibria at the inner and outer surfaces of the vesicles.

Based on such calibration, the fluorescence quenching signals could be converted into transmembrane ΔpH values. An absolute quantification of proton fluxes would in addition require knowledge of the values of the internal volume and buffer capacity of the vesicles. However, under the reasonable assumptions that these two parameters remain constant when the external ATP, ADP and P_i concentrations are varied, the approach allows an accurate quantification of the relative coupling ratios as a function of such concentrations. In the present work, the relative coupling ratio as a function of ATP concentration has not been explicitly calculated, but from Fig. 4C it is evinced to be constant at least up to 100 μM. Such constant value was expected, and it served as a negative control. Remarkably, when the same measurements and calculations were made as a function of P_i and ADP concentrations, the coupling ratios were found to change by up to a factor of 1.7 upwards (Fig. 7A) and a factor of 5 downwards, respectively (Fig. 7B). Since the 100% values of the two sets of data coincide, a combined factor of 8.5 is obtained. This is the highest value we have obtained experimentally, measured at the lowest calculated ADP concentration of 13 nM, but it should be considered that, in principle, even lower ADP concentrations could have been reached at higher PK concentrations. Both in Fig. 7B and in Fig. 5F, from which the former was derived, the fitting curve can indeed be extrapolated to lower values, not excluded the extreme value of zero. In other words, the present data are consistent with the possibility that an ATP synthase totally deprived of tightly bound ADP is also totally uncoupled.

The plots in Fig. 5F, in particular the biphasic one of $\Delta ATP/\Delta t$, indicate the involvement of two ADP binding sites, one at very high apparent affinity (about 30 nM), whose occupancy by ADP enhances the coupling ratio, and one at lower apparent affinity, in the submicromolar range, whose occupancy inhibits the hydrolysis activity. It should be noted that the presence in our assays of 50 μM ATP, a likely competitor for the same site, points to an even higher binding strength for ADP alone. The data obtained in our previous work in inverted *E. coli* membranes [28] did not allow to resolve two sites in the case of ADP, but only pointed to a site with apparent affinity in the submicromolar range.

The involvement of two ADP binding sites, affecting either the coupling ratio or the hydrolytic activity, parallels the involvement of two P_i binding sites (Fig. 3F), of which one affected the coupling ratio, and the other inhibited the hydrolytic activity. An apparent K_d of about 500 μM could be estimated for the latter, and a lower apparent K_d value in the tens of micromolar range could be estimated for the former (Fig. 7A). In the previous work in *E. coli* inverted membrane, the apparent K_d value for inhibition of hydrolysis was shown to increase at increasing PK concentration in the reaction assay, i.e. at decreasing amount of tightly bound ADP. This dependency on bound ADP could explain the higher value we have found in the isolated and reconstituted enzyme (510 μM) relative to the enzyme in inverted membranes (140 μM), if such enzyme had a higher content of bound ADP than the isolated and reconstituted one. Such a higher K_d value compares well with the one obtained in the isolated and reconstituted EF_1F_0 (apparent $K_d = 500$ μM) under deenergized conditions [44]. The occurrence of two P_i binding sites has been shown in the isolated EF_1 by direct binding studies, and the resulting K_d (at pH 7.5) were both estimated to be in the range of 0.1 mM [47].

The question is open as to whether these two sites are both catalytic. Two types of catalytic ADP binding sites, showing different affinities (with estimated K_d of 0.18 and 13 μM respectively), have been identified in an EF_0F_1 in which Trps introduced through mutagenesis into the catalytic sites were used as fluorescence reporters of nucleotide binding [48]. On the other hand, since very little is known about the properties of the non catalytic sites, it can not be totally excluded that the site, which in the present work shows the higher affinity for ADP, and is related to uncoupling but not to hydrolysis inhibition, is a non catalytic one.

On the whole, the results of the present work corroborate the idea that, in the ATP synthases, a mechanism has to exist which is able to change the coupling ratio of the pump according to the occupancy state

of one high affinity binding site for ADP and P_i, either catalytic or non catalytic, possibly reducing such coupling ratio to zero when the site is totally empty. On the nature of such mechanism it can only be speculated. It is possible to imagine that the occupancy of that site, through long-range conformational changes, is sensed at some stator/rotor interface, either in F_1 or in F_0, letting the rotor slide against the stator without energy transmission, or even at some rotor/rotor junction, which could loosen up, becoming the site of energy waste. The existence of uncoupling mutations e.g. at the γ/β interface [49], or at the ε/c interface [50] lends some experimental support to this possibility.

Alternatively, it could be the forced removal of ADP from catalytic sites which could lead to an uncoupled hydrolysis reaction, altering the ordinate event sequence required for the alternate binding mechanism. Two of us have recently presented a model, based on the available crystallographic structures of bovine and yeast F_1, considering the possibility that the phenomena studied in this work are related to the activity of the catalytic sites [51]. In that model it is suggested that the low affinity site could coincide with the pre-dissociation site for the hydrolysis product (the HC (half closed) conformation). The inhibition of hydrolysis by high P_i concentrations could be explained if dissociation of product P_i is reversed by medium P_i, thereby inhibiting the emptying of site for ATP binding. The absence of P_i inhibition in the presence of an ADP-trapping by PK is consistent with the synergistic effects of ADP in P_i binding. The second, higher affinity, site, that has to be occupied by both ADP and P_i in order to obtain a properly coupled hydrolysis cycle, is proposed to coincide with a conformation intermediate between the β_{TP} and β_{DP} ones, and similar to the ADP-AlF_4^- transition conformation. When this site is empty, due to omission of P_i from the reaction medium and to the addition of a very active ADP-trapping system, a futile uncoupled hydrolysis cycle is proposed to occur, during which ATP is bound and hydrolyzed, and ADP and P_i are released while this site oscillates in the synthesis and hydrolysis direction, not leading to any net rotation.

An additional open question is whether such intrinsic uncoupling of the ATP synthase has a physiological role in the bacterial cell. It seems plausible that such a crucial parameter like the coupling ratio of the ATP synthase might be advantageously kept elastic and subjected to regulation. While the intracellular P_i concentration in *E. coli* has been estimated in a range (see e.g. [52]) which would suit the K_d value we have found, the K_d value found for ADP is obviously too small compared to the ADP concentrations in vivo. However, it is not unlikely that such site not only binds ADP but also, competitively, ATP, and it could be consequently envisaged that it is rather the ratio ATP/ADP which determines the actual coupling ratio. Moreover, an additional and still largely unexplored issue is whether also the protonmotive force can influence the coupling ratio, as it is the case in the V-ATPases [23,26] and cytochrome oxidases (reviewed in [53]). These questions may be clarified in future work.

Acknowledgements

We thank Stan Dunn and Giovanni Venturoli for insightful discussions. This work has been supported by the grant PRIN Project number 2005052128_004 from the Italian Ministry for Education, University and Research (MIUR).

Appendix

The internal buffering power in reconstituted vesicles.

The conventional definition of internal buffering capacity of vesicles is:

$$\beta\left(\left[H^+\right]_{in}\right) = dpH_{in} / dn_{H^+} \tag{A1}$$

where $\beta([H^+]_{in})$ is the internal buffering capacity (which can be contributed both by endogenous buffers, like protein and lipid head groups, and by soluble buffers in the bulk phase), Δn_{H^+} is the amount of protons transferred into the inner lumen, and ΔpH_{in} the ensuing change in internal pH. The two quantities are not linearly related at variable $[H^+]_{in}$, since $\beta([H^+]_{in})$ is an implicit function of the internal proton concentration $[H^+]_{in}$.

The behaviour of the internal buffering capacity can be modelled by a summation of buffers, whose concentrations and pK_as describe adequately the internal buffering phenomena [54]. In this case the relation between the rate of proton influx and the rate of inner proton concentration can be explicitly described as follows:

$$dn_{H^+}/dt = V_{in} \cdot d\left(\left[H^+\right]_{in}\left(1 + \sum_i\left(A_i\Big/\left(\left[H^+\right]_{in} + K_i\right)\right)\right)/dt \tag{A2}$$

or, calculating the derivative of the second member:

$$dn_{H^+}/dt = V_{in} \cdot d\left[H^+\right]_{in}\Big/dt\left(1 + \sum_i\left(A_iK_i\Big/\left(\left[H^+\right]_{in} + K_i\right)^2\right)\right) \tag{A3}$$

where V_{in} is the vesicle inner volume, and A_i and K_i are respectively the concentration and proton dissociation constant of the *i*-th buffer in the summation. By posing $\boldsymbol{B}([H^+]_{in}) = (1+\sum_i (A_iK_i/([H^+]_{in}+K_i)^2)$, Eq. (A3) can be written as

$$dn_{H^+}/dt = V_{in} \cdot B\left(\left[H^+\right]_{in}\right) \cdot d\left[H^+\right]_{in}\Big/dt \tag{A4}$$

which emphasizes the fact that, for each given $[H^+]_{in}$ value, the rate of inward proton translocation is proportional to the rate of acidification of the inner compartment, and that the proportionality constant is a function of the buffering power of the system at a given $[H^+]_{in}$.

Eq. (A2) can also be integrated, when necessary [54]. Usually, the number of buffers needed for a suitable simulation and their concentrations and K_as are unknown. These parameters can be determined in experiments where the influx rate of protons is known and the internal concentration changes are measured [55]. In the present work, on the other hand, the rates of change of $[H^+]_{in}$ were evaluated within a given concentration interval, kept equal for all conditions, and compared to a reference condition, so that the amount of buffered protons was the same in each case, and could be ignored.

References

[1] P.D. Boyer, The ATP synthase—a splendid molecular machine, Annu. Rev. Biochem. 66 (1997) 717–749.
[2] M. Yoshida, E. Muneyuki, T. Hisabori, ATP synthase—a marvelous rotary engine of the cell, Nat. Rev. Mol. Cell Biol. 2 (2001) 669–677.
[3] J. Weber, A.E. Senior, ATP synthesis driven by proton transport in F_1F_0-ATP synthase, FEBS Lett. 545 (2003) 61–70.
[4] K. Kinosita Jr., K. Adach, H. Itoh, Rotation of F1-ATPase: how an ATP-driven molecular machine may work, Annu. Rev. Biophys. Biomol. Struct. 33 (2004) 245–268.
[5] S. Wilkens, Rotary molecular motors, Adv. Protein Chem. 71 (2005) 345–382.
[6] J.P. Abrahams, A.G. Leslie, R. Lutter, J.E. Walker, Structure at 2.8 Å resolution of F1-ATPase from bovine heart mitochondria, Nature 370 (1994) 621–628.
[7] P.D. Boyer, W.E. Kohlbrenner, The present status of the binding-change mechanism and its relation to ATP formation by chloroplasts, in: B.R. Selman, S. Selman-Reimer (Eds.), Energy Coupling in Photosynthesis, Elsevier North Holland, New York, 1981, pp. 231–240.
[8] P.D. Boyer, The binding change mechanism for ATP synthase—some probabilities and possibilities, Biochim. Biophys. Acta 1140 (1993) 215–250.
[9] K. Braig, R.I. Menz, M.G. Montgomery, A.G. Leslie, J.E. Walker, Structure of bovine mitochondrial F(1)-ATPase inhibited by Mg(2+) ADP and aluminium fluoride, Structure 8 (2000) 567–573.
[10] R.I. Menz, J.E. Walker, A.G. Leslie, Structure of bovine mitochondrial F(1)-ATPase with nucleotide bound to all three catalytic sites: implications for the mechanism of rotary catalysis, Cell 106 (2001) 331–341.
[11] R. Kagawa, M.G. Montgomery, K. Braig, A.G. Leslie, J.E. Walker, The structure of bovine F_1-ATPase inhibited by ADP and beryllium fluoride, EMBO J. 23 (2004) 2734–2744.
[12] M.W. Bowler, M.G. Montgomery, A.G. Leslie, J.E. Walker, How azide inhibits ATP hydrolysis by the F-ATPases, Proc. Natl Acad. Sci. USA 103 (2006) 8646–8649.

[13] G. Groth, E. Pohl, The structure of the chloroplast F_1-ATPase at 3.2 A resolution, J. Biol. Chem. 276 (2001) 1345–1352.
[14] A.C. Hausrath, R.A. Capaldi, B.W. Matthews, The conformation of the epsilon- and gamma-subunits within the *Escherichia coli* F(1) ATPase, J. Biol. Chem. 276 (2001) 47227–47232.
[15] V. Kabaleeswaran, N. Puri, J.E. Walker, A.G. Leslie, D.M. Mueller, Novel features of the rotary catalytic mechanism revealed in the structure of yeast F_1 ATPase, EMBO J. 25 (2006) 5433–5442.
[16] D. Pietrobon, S.R. Caplan, Flow–force relationships for a six-state proton pump model: intrinsic uncoupling, kinetic equivalence of input and output forces, and domain of approximate linearity, Biochemistry 24 (1985) 5764–5776.
[17] A. Baccarini Melandri, R. Casadio, B.A. Melandri, Thermodynamics and kinetics of photophosphorylation in bacterial chromatophores and their relation with the transmembrane electrochemical potential difference of protons, Eur. J. Biochem. 78 (1977) 389–402.
[18] D. Branca, S.J. Ferguson, M.C. Sorgato, Clarification of factors influencing the nature and magnitude of the protonmotive force in bovine heart submitochondrial particles, Eur. J. Biochem. 116 (1981) 341–346.
[19] B.A. Bulthuis, G.M. Koningstein, A.H. Stouthamer, H.W. van Verseveld, The relation of proton motive force, adenylate energy charge and phosphorylation potential to the specific growth rate and efficiency of energy transduction in *Bacillus licheniformis* under aerobic growth conditions, Antonie Leeuwenhoek 63 (1993) 1–16.
[20] K. Olsson, S. Keis, H.W. Morgan, P. Dimroth, G.M. Cook, Bioenergetic properties of the thermoalkaliphilic Bacillus sp. strain TA2.A1. J. Bacteriol. 185 (2003) 461–465.
[21] D.J. Cipriano, Y. Bi, S.D. Dunn, Genetic fusions of globular proteins to the epsilon subunit of the *Escherichia coli* ATP synthase: implications for in vivo rotational catalysis and epsilon subunit function, J. Biol. Chem. 277 (2002) 16782–16790.
[22] D.J. Cipriano, S.D. Dunn, The role of the epsilon subunit in the *Escherichia coli* ATP synthase. The C-terminal domain is required for efficient energy coupling, J. Biol. Chem. 281 (2006) 501–507.
[23] J.M. Davies, I. Hunt, D. Sanders, Vacuolar H(+)-pumping ATPase variable transport coupling ratio controlled by pH, Proc. Natl Acad. Sci. USA 91 (18) (1994 Aug 30) 8547–8551.
[24] M.L. Müller, M. Jensen, L. Taiz, The vacuolar H + -ATPase of lemon fruits is regulated by variable H^+/ATP coupling and slip, J. Biol. Chem. 274 (1999) 10706–10716.
[25] M.L. Müller, L. Taiz, Regulation of the lemon-fruit V-ATPase by variable stoichiometry and organic acids, J. Membr. Biol. 185 (2002) 209–220.
[26] C. Kettner, A. Bertl, G. Obermeyer, C. Slayman, H. Bihler, Electrophysiological analysis of the yeast V-type proton pump: variable coupling ratio and proton shunt, Biophys. J. 85 (2003) 3730–3738.
[27] P. Turina, D. Giovannini, F. Gubellini, B.A. Melandri, Physiological ligands ADP and P_i modulate the degree of intrinsic coupling in the ATP synthase of the photosynthetic bacterium *Rhodobacter capsulatus*, Biochemistry 43 (2004) 11126–11134.
[28] M. D'Alessandro, P. Turina, B.A. Melandri, Intrinsic uncoupling in the ATP synthase of *Escherichia coli*, Biochim. Biophys. Acta 1777 (2008) 1518–15127.
[29] Y. Moriyama, A. Iwamoto, H. Hanada, M. Maeda, M. Futai, One-step purification of *Escherichia coli* H^+-ATPase (F_0F_1) and its reconstitution into liposomes with neurotransmitter transporters, J. Biol. Chem. 266 (1991) 22141–22146.
[30] S. Fischer, C. Etzold, P. Turina, G. Deckers-Hebestreit, K. Altendorf, P. Gräber, ATP synthesis catalyzed by the ATP synthase of *Escherichia coli* reconstituted into liposomes, Eur. J. Biochem. 225 (1994) 167–172.
[31] M.M. Bradford, A rapid and sensitive method for the quantitation of microgram quantities of protein utilizing the principle of protein-dye binding, Anal. Biochem. 72 (1976) 248–254.
[32] S. Fischer, P. Gräber, Comparison of ΔpH- and Δφ- driven ATP synthesis catalyzed by the H^+-ATPases from *Escherichia coli* or chloroplasts reconstituted into liposomes, FEBS Lett. 457 (1999) 327–332.
[33] P. Richard, J.L. Rigaud, P. Gräber, Reconstitution of CF_0F_1 into liposomes using a new reconstitution procedure, Eur. J. Biochem. 193 (1990) 921–925.
[34] P.W. Holloway, A simple procedure for removal of Triton X-100 from protein samples, Anal. Biochem. 53 (1973) 304–308.
[35] M. Nishimura, T. Ito, B. Chance, Studies on bacterial photophosphorylation. III. A sensitive and rapid method of determination of photophosphorylation, Biochim. Biophys. Acta 59 (1962) 177–182.
[36] P.A. Lanzetta, L.J. Alvarez, P.S. Reinach, O.A. Candia, An improved assay for nanomole amounts of inorganic phosphate, Anal. Biochem. 100 (1979) 95–97.
[37] R. Casadio, B.A. Melandri, Calibration of the response of 9-amino acridine fluorescence to transmembrane pH differences in bacterial chromatophores, Arch. Biochem. Biophys. 238 (1985) 219–228.
[38] H. Ruf, Y. Georgalis, E. Grell, Dynamic laser light scattering to determine size distributions of vesicles, Meth. Enzymol. 172 (1989) 364–390.
[39] R. Rottler, Fluorescence spectroscopy studies on the H^+-ATPase from chloroplasts and on the transmembrane proton fluxes in proteoliposomes. Ph.D. Thesis, University of Stuttgart (2002).
[40] J.F. Nagle, M.C. Wiener, Structure of fully hydrated bilayer dispersions, Biochim. Biophys. Acta 942 (1988) 1–10.
[41] B. Zimmermann, M. Diez, N. Zarrabi, P. Gräber, M. Börsch, Movements of the epsilon-subunit during catalysis and activation in single membrane-bound H(+)-ATP synthase, EMBO J. 24 (2005) 2053–2063.
[42] S. Schuldiner, H. Rottenberg, M. Avron, Determination of pH in chloroplasts. 2. Fluorescent amines as a probe for the determination of pH in chloroplasts, Eur. J. Biochem. 25 (1972) 64–70.
[43] R. Casadio, Measurements of transmembrane pH differences of low extents in bacterial chromatophores, Eur. Biophys. J. 19 (1991) 189–201.
[44] S. Fischer, P. Gräber, P. Turina, The activity of the ATP synthase from *Escherichia coli* is regulated by the transmembrane proton motive force, J. Biol. Chem. 275 (2000) 30157–30162.
[45] B.A. Feniouk, M. Yoshida, The role of subunit e in the catalysis and regulation of F_0F_1-ATP synthase, Biochim. Biophys. Acta 1757 (2008) 326–338.
[46] P. Turina, B. Rumberg, B.A. Melandri, P. Gräber, Activation of the H(+)-ATP synthase in the photosynthetic bacterium *Rhodobacter capsulatus*, J. Biol. Chem. 267 (1992) 11057–11063.
[47] H.S. Penefsky, P_i binding by the F1-ATPase of beef heart mitochondria and of the *Escherichia coli* plasma membrane, FEBS Lett. 579 (2005) 2250–2252.
[48] S. Löbau, J. Weber, A.E. Senior, Catalytic site nucleotide binding and hydrolysis in F1F0-ATP synthase, Biochemistry 37 (1998) 10846–10853.
[49] Y. Wang, U. Singh, D.M. Mueller, Mitochondrial genome integrity mutations uncouple the yeast *Saccharomyces cerevisiae* ATP synthase, J. Biol. Chem. 282 (2007) 8228–8236.
[50] Y. Zhang, M. Oldenburg, R.H. Fillingame, Suppressor mutations in F1 subunit epsilon recouple ATP-driven H + translocation in uncoupled Q42E subunit c mutant of *Escherichia coli* F1F0 ATP synthase, J. Biol. Chem. 269 (1994) 10221–10224.
[51] M. D'Alessandro, B.A. Melandri, Biochim. Biophys. Acta 1797 (2010) 755–762.
[52] K. Ugurbil, H. Rottenberg, P. Glynn, R.G. Shulman, Phosphorus-31 nuclear magnetic resonance studies of bioenergetics in wild-type and adenosinetriphosphatase(1-) *Escherichia coli* cells, Biochemistry 21 (1982) 1068–1075.
[53] B. Kadenbach, Intrinsic and extrinsic uncoupling of oxidative phosphorylation, Biochim. Biophys. Acta 1604 (2003) 77–94.
[54] J. Whitmarsh, Proton decay kinetics for vesicles containing buffers—an analytical solution, Photosynth. Res. 12 (1987) 43–62.
[55] P. Turina, G. Venturoli, B.A. Melandri, Evaluation of the buffer capacity and permeability constant for protons in chromatophores from *Rhodobacter capsulatus*, Eur. J. Biochem. 192 (1990) 39–47.